

UNIVERSITÀ DEGLI STUDI DI PADOVA

DEPARTMENT OF INDUSTRIAL ENGINEERING
MASTER'S DEGREE IN MATERIAL ENGINEERING

**Master's Thesis in
Materials Engineering**

**WEAR BEHAVIOUR OF Ti6Al4V FEMORAL HEAD
SURFACES FUNCTIONALIZED THROUGH ULTRASONIC
VIBRATION TURNING FOR DRUG DELIVERY**

Supervisor: Prof. Stefania Bruschi

Co-supervisor: Dr. Rachele Bertolini

Student: LUCIA LIZZUL

ACADEMIC YEAR 2017/2018

ACKNOWLEDGEMENTS

I would like to thank Professor Bruschi Stefania for giving me this opportunity and for believing in my potential from the beginning.

A special thanks goes to Rachele whose tenacity and hardworking inspired me and helped me to complete this project.

INDEX

ABSTRACT	1
RIASSUNTO	3
1 INTRODUCTION	5
1.1 Medical implants overview	5
1.2 Materials for medical implants	5
<i>1.2.1 Materials for orthopaedic applications</i>	<i>7</i>
1.3 Hip joint arthroplasty	9
<i>1.3.1 Hip joint anatomy</i>	<i>9</i>
<i>1.3.2 Hip joint prosthesis</i>	<i>11</i>
1.4 Material selection for femoral head and stem	13
<i>1.4.1 Materials specific requirements</i>	<i>13</i>
<i>1.4.2 Common materials for femoral head and stem</i>	<i>14</i>
<i>1.4.3 Introduction to Titanium</i>	<i>15</i>
<i>1.4.3.1 Titanium crystal structure</i>	<i>16</i>
<i>1.4.3.2 Corrosion resistance</i>	<i>16</i>
<i>1.4.3.3 Ti6Al4V</i>	<i>17</i>
1.5 Manufacturing technique for metal prosthesis – EBM	20
1.6 Engineered surfaces	21
<i>1.6.1 Applications</i>	<i>21</i>
1.7 Engineered surfaces technologies	23
<i>1.7.1 Adding material technologies</i>	<i>24</i>
<i>1.7.2 Removing material technologies</i>	<i>24</i>
<i>1.7.2.1 Chemical texturing</i>	<i>25</i>
<i>1.7.2.2 Mechanical texturing</i>	<i>25</i>

1.7.3 <i>Moving material technologies</i>	25
1.7.4 <i>Self-forming technologies</i>	26
1.8 Advances in materials functionalization	27
1.9 Introduction to Ultrasonic Vibration Turning	29
1.9.1 <i>Summary of different type of UVT</i>	30
1.9.2 <i>Servo designs</i>	31
1.9.3 <i>Kinematics of vibration-assisted machining</i>	33
1.9.4 <i>One-dimensional vibration-assisted machining</i>	34
1.9.5 <i>Two-dimensional vibration-assisted machining</i>	36
1.10 Tribology	40
1.10.1 <i>History and beginnings</i>	40
1.10.2 <i>Friction</i>	41
1.10.3 <i>Wear</i>	41
1.10.3.1 <i>Classification of wear mechanisms</i>	42
1.10.4 <i>Lubrication</i>	43
1.10.4.1 <i>Lubrication regimes</i>	44
1.11 Hip prosthesis as a tribological system	46
1.11.1 <i>Hertz contact theory</i>	47
1.11.2 <i>Cylinder-on-plane contact</i>	48
2 EXPERIMENTAL SECTION	50
2.1 Materials	50
2.2 Machining	52
2.3 Microstructural and mechanical characterization after machining	53
2.4 Contact angle measurements	54
2.5 Surface topography analysis after machining	54

2.6 Wear tests	55
2.6.1 Setup design	56
2.6.2 Wear test parameters	58
2.7 Characterization after wear tests	60
3 RESULTS AND DISCUSSION	61
3.1 Microstructural and mechanical characteristics of the machined samples	61
3.2 Wettability results	62
3.3 Surface topography before and after wear	63
3.4 Tribological results	66
3.5 SEM images of wear scars	69
4 CONCLUSIONS	72
5 LIST OF ABBREVIATIONS	75
6 BIBLIOGRAPHY	77

ABSTRACT

Total hip replacements often need a premature postoperative revision due to a flare of the body's inflammatory response, which may be limited if suitable drugs are delivered on site as a function of time. To this aim, the femoral head surface may be functionalized realizing textures that can be exploited as potential reservoir of drugs.

Ultrasonic Vibration Turning (UVT) is used in this work to generate texturized surfaces on Ti6Al4V cylinders through a high frequency alternative motion given to the cutting tool. By varying the cutting parameters, micro-dimples of different geometrical characteristics, orthogonal to the feed direction, are formed on the surface. The surface valleys so generated, could be possible sites to store drugs able to act against infection onset.

In vitro pin-on-disc wear tests are carried out to prove the surface texturing does not lead to a worsening of the wear resistance compared to polished surfaces, currently used for commercial femoral heads.

In this introductory work the Ti6Al4V UVTed cylinders are made to slide against UHMWPE (ultra-high molecular weight polyethylene) discs in a circular path reproducing the physiological conditions. For sake of comparison, Ti6Al4V polished cylinders are also tested.

It is shown that the presence of the micro-dimples induced by UVT alters neither the microstructure nor the hardness of the Ti6Al4V cylinders, whereas the surface topography is drastically modified without affecting negatively the wear performances compared to the standard polished surfaces.

To this regard, UVT appears to be a promising manufacturing technique to functionalize the surface of artificial femoral heads through the creation of micro-dimples for drug delivery during the first stages of the prosthetic implantation, without affecting the wear performances of the implant itself.

RIASSUNTO

La sostituzione totale dell'anca spesso richiede una revisione post-operatoria prematura in seguito ad una riacutizzazione della risposta infiammatoria da parte dell'organismo. Tale inconveniente può essere limitato grazie al rilascio *in situ* di opportuni medicinali. A tale scopo, la superficie delle teste femorali artificiali può essere funzionalizzata mediante tecniche innovative di asportazione di truciolo che modificano l'integrità superficiale del componente, realizzando una microstruttura che può essere sfruttata come potenziale sede di immagazzinamento di medicinale. In questo progetto di tesi viene utilizzata l'*Ultrasonic Vibration Turning* (UVT) per lavorare la superficie di cilindri in Ti6Al4V attraverso un movimento alternato ad alta frequenza dell'utensile di taglio. Variando i parametri di taglio è stato possibile generare sulla superficie del metallo delle micro-buche, ortogonali alla direzione di avanzamento, con diverse caratteristiche geometriche. Le valli superficiali così generate potrebbero fungere da siti di immagazzinamento di medicinale in grado di agire contro l'infiammazione. Sono state dunque condotte delle prove di usura *pin-on-disc* al fine di verificare che la presenza di micro-buche superficiali indotte dall'UVT non alteri l'entità dell'usura nelle protesi rispetto all'attuale configurazione adottata, in cui la superficie del titanio viene lucidata a specchio. Dei cilindri di Ti6Al4V lavorati con l'UVT sono stati fatti slittare su dei dischi di UHMWPE (*ultra-high molecular weight polyethylene*) con un moto di tipo circolare, riproducendo così l'ambiente e le sollecitazioni che gli impianti femorali sperimentano *in vivo*. Come confronto, i test sono stati effettuati anche su cilindri in Ti6Al4V lucidati. Dalle analisi condotte risulta che la presenza delle micro-buche indotte dall'UVT non alteri né la microstruttura né la microdurezza dei cilindri di Ti6Al4V, nonostante la drastica modificazione della topografia superficiale. Dai risultati delle prove di usura si evince che non vi sono peggioramenti nell'utilizzo di una superficie lavorata con l'UVT rispetto a una lucidata.

In conclusione, si può affermare che l'UVT possa essere una promettente tecnica di asportazione del truciolo per funzionalizzare la superficie di teste femorali protesiche ed essere una potenziale alternativa che permetta di risolvere l'infiammazione nei primi stadi post-operatori grazie al *drug delivery*.

1 INTRODUCTION

1.1 Medical implants overview

In the recent years an increased life expectancy has been reached worldwide [1], coupled with a growth of medical devices implantology such as artificial pacemakers, coronary stents, neurostimulator, drug delivery systems and orthopaedics implants and so on [2]. The target of an implant is to treat or to replace a malfunctioning tissue or organ of a human body [3]. The sector that gained the largest market and the most flourishing is the orthopaedics one. This fact is mostly linked to the rising of obesity, osteoarthritis and degenerative joint diseases in developed countries [4] in addition to the better healthcare in developing countries like China and India [5]. In general, there is a growing consciousness about the advantages of such surgeries and the better quality of life it brings. Only in the US, over 300,000 total hip replacements are carried out annually [6]. Moreover, literature it is possible to find projection studies that report increases in number of total hip arthroplasty (THA) and total knee arthroplasty (TKA) always greater than 50% in the next fifteen years [7]–[9].

In this scenario, there is a strong need for efficient, long-lasting and patient-specific prosthesis, trying to avoid an immune system rejection.

The most important feature determining the success of an implant is its material.

1.2 Materials for medical implants

In the last decades lot of materials, able to withstand physiological conditions and biological environment, have been investigated [10]–[13]. They can be commonly divided into four main categories, depending on the chemistry nature: metals, ceramics, polymers and composites [14].

Materials for biological applications have to undergo some crucial aspects. First, they have to be biocompatible, denoting that it should not interfere harmfully with normal physiological activities [15]. An ideal biocompatible material should be characterized by a good chemical stability, non-toxicity, non cancerogenicity, hemocompatibility, no immunogenicity and non-irritability in order to prevent

undesired host tissue response [3]. To evaluate the biocompatibility of a certain material it should be considered also the shape, the location of the implant and its duration, the presence of additives and the nature of potential degradation products. A medical implant can be considered successful if the materials it is made of, interact favorably with the surrounding tissues. Depending on the extent of these interactions, a biomaterial can be divided into bioinert, bioactive or bioresorbable. In the first case, the interaction is minimal, allowing for a good coexistence between the organism and the implant. Examples of bioinert material are titanium, tantalum, alumina and zirconia, ultra-high molecular weight polyethylene. Bioactive materials promote direct biochemical interactions with the biological tissue, which can grow on the material surface itself. This allows for a solid mechanical bond between the natural tissue and the implant. Materials belonging to this class are hydroxyapatite and Bioglass[®] [16]. Bioresorbable materials undergo a progressive degradation into the biological system, without eliciting immune rejection or toxic effects. Typical bioresorbable materials are calcium triphosphate, porous hydroxyapatite and some kind of Bioglass[®]. Bioresorbable materials can also be bioactive such as copolymers of lactic acid or of glycolic acid, allowing for a gradual replacing by the biological tissue. This kind of material is usually utilized for drug delivery systems.

Stated that, it is clear that the material choice and design depend strictly on the final purpose of the implant and on its location in the body.

Beside the material chemistry, it is crucial to considerate materials mechanical properties. Thanks to their unique mechanical properties and processability, metals are the most utilized material for medical implants (over 70% of all medical implants [17]), even if technological progresses have been made in other material classes. The most important characteristics that makes metals suitable for many biomedical applications are the capacity of bearing high loads without large elastic and plastic deformation; moreover, its ductility avoids fragile behavior.

1.2.1 Materials for orthopaedic applications

The most important mechanical properties necessary for orthopaedic implants are the following:

- strength – in order to bear high stresses to which bones are subjected, for instance, the hip joints can bear a load up to ten times the body weight [18];
- fracture toughness – to not fracture in its service life;
- ductility – to avoid brittle fracture that is sudden and unpredictable;
- fatigue life – to withstand the cyclicity of loading experienced by bones during the body motion;
- wear resistance – to contain the debris formation during sliding of two or more components and thus avoiding the elicitation of an acute inflammation;
- corrosion resistance – to avoid the releasing of toxic substances into the body.

The material class that most of all satisfies these properties is that one of metals. As already stated in the previous paragraph, metals are characterized by a high strength and fracture toughness, moreover they are ductile and mostly with a high fatigue limit. The major drawbacks of metals are their corrosion and wear resistance. Human body fluids are highly corrosive towards metals, since they are quite warm, contain oxygen and about 1% w/w of NaCl beside other salts in lower concentrations. Therefore, they can lead to generalized corrosion beside interstitial corrosion, pitting, fretting, tensile-corrosion and corrosion for fatigue [19]. During corrosion metal ions are released with two consequences, first the loss of implant functionality due to the mechanical properties worsening, secondly tissue contamination by the ions toxicity with serious damages to the patient's health. Moreover, metals are too rigid respect to the human bone. Cortical bone is characterized by a Young's modulus of about 20 up to 40 GPa, that is an order of magnitude lower than biometals. This brings to a change in the stress distribution and, since the bone is no more loaded and stimulated, it stops to remodel losing density and thus weakening becoming more fragile [20]. This is the so-called stress shielding and it is one of the most common reasons of long-term implant failure. Finally, metals for implants do not have to be magnetic, since their presence in the patient body would lead to an interference with the magnetic field utilized in the

magnetic resonance spectroscopy for diagnostic For this reason, metals that must be avoided are ferritic and martensitic stainless steel and alloys with high nickel and/or cobalt content [21].

Metals utilized for orthopaedic applications are Co–Cr–Mo alloys, commercially pure Ti, grade 4 Ti, Ti6Al4V and in minor extent stainless steel (316, 316L) , NiTi alloys, tantalum and magnesium alloys for bioresorbable implants [22].

For what concerns polymers, they are claimed to have good biocompatibility. However, some of them lose much of their resistance, already poor, once implanted in vivo. There is a high risk of debris releasing caused by wear or monomer releasing due to chemical degradation or uncompleted polymerization. Generally, polymers cannot bear high loads, tend to swell and leak fillers and antioxidants. Furthermore they are difficult to sterilize without affecting their properties [22]. Some of polymeric biomaterials used in orthopaedic applications are poly(methyl methacrylate) (PMMA) as bone cements, ultra-high molecular weight polyethylene (UHMWPE) for acetabular cups in artificial hip joint and patellar components in artificial knee replacements, polydimethylsulphoxide (PDMS) for small joints in hand and foot, polyetheretherketone (PEEK) for spinal implants.

Ceramics in orthopaedics are used due to their outstanding biocompatibility, exceptional corrosion resistance and good frictional properties [23]. They are mostly utilized in total hip replacements as femoral heads and /or as acetabular cups. These materials are characterized by high strength, but they are brittle and difficult to manufacture. For the application over mentioned alumina and zirconia ceramics are the most utilized. Calcium phosphate ceramics such as hydroxyapatite and tricalcium phosphate are commonly used as coating for bone fixation in substitution to classical cemented prostheses. The capability to bond chemically to the bone is possible due to their composition comparable to the mineral bone one [24].

Finally, also composites materials are utilized for orthopaedic applications. Compared to homogeneous materials, composites can offer better performances with a high control on properties, depending on the design. The most common matrix in composites is the polymeric one. In fact, the polymeric matrix shows an isoelastic behaviour, having a comparable stiffness to the bone, reducing stress-shielding issue [25]. However, when utilizing composites for biomedical applications it is important to assess that each component is biocompatible and to verify that the interface of constituents do not represent a weak region to the body

fluids attack. Various matrix-reinforcement combinations are possible, some examples are carbon fiber reinforced polyetheretherketone [26], stainless-steel-fiber-reinforced Bioglass[®], polyethylene-hydroxyapatite [27].

1.3 Hip joint arthroplasty

Nowadays, THA became one of the most popular surgical operations. Patients suffering from hip pain can recover the function of the joint with consequent cessation of pain, achieving a better quality of life.

Since the 1960s, the British surgeon Sir John Charnley, considered the pioneer of the hip prosthesis, intensively devoted himself to the study of the biomechanics of hip joint. He tried to solve the major problems encountered in previous attempts to build prostheses. He focused mainly on the problems of lubrication and fixation of the hip prosthesis introducing for the first time the use of high molecular weight polyethylene and the idea of using bone cement [28]. Even today, his discoveries and the design of the prosthesis are the basis of the current implants.

It is possible to identify three fundamental reasons for the high incidence of THA surgeons:

- a. The hip joint is the one subject to the greatest loads, therefore the one that most frequently undergoes mechanical failures
- b. Hip replacement is rather simple surgically;
- c. Its kinematics can be easily reproduced using a spherical joint.

1.3.1 Hip joint anatomy

Joints are important parts of the skeletal system, located in correspondence of the conjunctions of the bones. Their function is to transmit loads among bones through muscle action; this effect it is generally accompanied by a relative movement of the component bones.

Osseous tissue is a hard tissue that can be seen as complex natural composite. It is primarily composed of a protein, the collagen, present as elastic fibers, offering

fracture resistance to the skeleton, and of an inorganic component, the bone mineral, that gives rigidity to the bone. The main mineral is a calcium phosphate, the hydroxyapatite (HA).

Bone tissue is anisotropic, since it has different properties in the longitudinal and transverse directions. **Table 1** summarizes the mechanical properties of cortical and cancellous bone. The first one is compact and dense, constitutes the hard outer layer of the bone. The second one is the internal part of the bone and has a spongy architecture with an open cell architecture giving lightness and elasticity to the bone.

Table 1 Mechanical properties of the two main types of bone tissues [29].

<i>Tissue</i>	<i>Density [g/cm³]</i>	<i>Compressive strength [MPa]</i>	<i>Tensile strength [MPa]</i>	<i>Elastic Modulus [GPa]</i>
<i>Cortical bone</i>	1.8-2.0	160 <i>trans.</i> 240 <i>long.</i>	35 <i>trans.</i> 283 <i>long.</i>	5-23
<i>Cancellous bone</i>	1.0-1.4	1.5-9.3	1.5-38	0.01-1.57

The human hip joint connects the lower limbs bones to the upper part of the skeleton through the pelvis. It is formed by the articulation of the spherical head of the femur and the cup-like cavity into the pelvis, called acetabulum. It allows a wide range of movements: flexion and extension movements on the sagittal plane, abduction and adduction on the frontal plane, rotation and circumduction. In **Figure 1** the anatomy of the hip joint is showed.

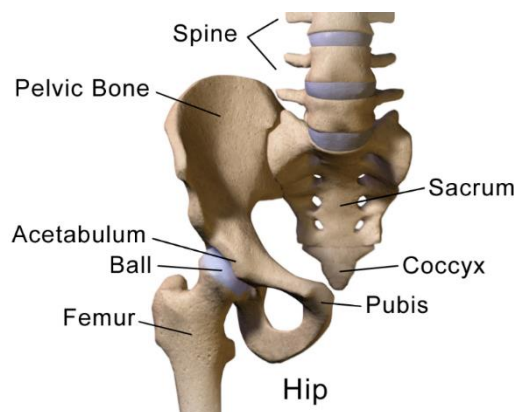


Figure 1 Human hip joint anatomy.

1.3.2 Hip joint prosthesis

Hip replacement can be total or a partial. This kind of surgery is usually performed to fix fractures or to relieve pain due to osteoarthritis. The fracture typically occurs in the narrow region just below the femoral head.

In case of osteoarthritis, small fragments of joint cartilage and of surrounding bone are released because of their breakdown. These fragments remain in the joint area, causing an inflammation with a consequent pain, joint effusion and loss of mobility.

Total hip replacement surgery involves the removal of the femoral head and of the upper part of the femur, as well as a part of the bone marrow internal to the upper remaining segment of the femur. A hole is thus created, in which the metal stem of the prosthesis will fit. In addition, also the cartilage and the bone of the pelvis acetabulum are removed to accommodate the artificial cup.

Modern hip prostheses are typically composed of four parts as shown in **Figure 2** adapted form [30]: a femoral stem, a spherical head, a liner and an acetabular cup. Different material and combinations are possible depending on the patients need and on the surgeon indications.

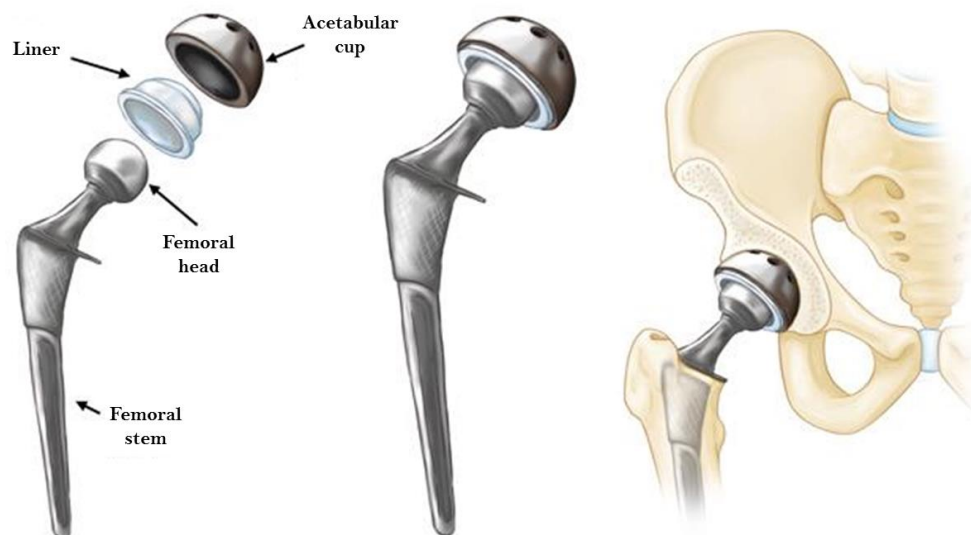


Figure 2 Hip joint prosthesis components. Adapted from [30].

The acetabular component is almost always composed of two parts: a metal shell and a liner that can be ceramic or in polyethylene. While the inner surface of the metal shell has a securing mechanism to fix the liner, the outer one has a porous coating. The latter allows for the cup fixation on the pelvis. At the beginning the firmness is achieved by the force of insertion, with time bone grows into the coating pores allowing for the integrating of the implant. Finally, screws may be utilized to assure additional fixation.

The femoral component is the part of the implant that is inserted into the femur. At the opposite side it has the spherical femoral head. To stabilize the femoral stem to the bone, there is the possibility to cement it or not. In the first case polymethylmethacrylate (PMMA), also known as bone cement, is utilized as adhesive. Uncemented femoral stems are fixed using friction together with a specific shape and surface finishing to stimulate the bone ingrowth and thus merging the implant to the bone. Femoral stems can be made of different materials such as stainless steel, cobalt chromium alloys, titanium alloys or polymer matrix composites.

Femoral components can be monolithic or modular. In the latter case various combinations of head size and neck orientation are possible, offering a wider adaptability to the patient anatomy. However, some complications can occur: if the implant components do not perfectly fit, it is possible to incur galvanic corrosion and/or wear of the involved parts. Comparing the two kind of femoral components it is possible to observe that the modular stem has 10-20% less mechanical resistance than the monobloc component. To avoid failure, the components must be machined with care, especially in the joint area, avoiding damaging during implantation. Moreover, particular attention should be taken in cleaning procedures.

For what concerns the femoral heads, they can be both metallic or ceramic. After machining, metal heads are polished to make them smooth. Ceramic heads offer even smoother surfaces than polished metal and it was thought that this feature would help the reduction of wear, but recent studies do not confirm this theory. Moreover, ceramic heads are more fragile and more prone to break once implanted. The femoral head articulates with the acetabulum, forming the so-called ball on socket joint, reproducing the real articulation variety of motion. Also in this case, various sizes, materials and tolerances are feasible to produce an implant suitable

for the specific case. Common sizes for femoral heads range from 22 to 40 mm. The bigger the diameter, the lower the dislocation risk, allowing for an improved stability. On the other hand, larger femoral heads lead to higher friction and inertia. Currently the most common and preferred solution is metal-on-polyethylene (MOP) articular interface. This option consists of a metal shell and of a UHMWPE liner. Metal-on-crosslinked polyethylene (MOXP) pairing is gaining increasingly attention lately as well. Other typical coupling materials are metal on metal (MOM) and ceramic on ceramic (COC). Each pair has its benefits and drawbacks.

1.4 Material selection for femoral head and stem

This paragraph is dedicated to the specific requirements for artificial femoral head and stem materials in hip prostheses. Later, these materials will be discussed.

1.4.1 Materials specific requirements

Bones and hip prosthesis components transmit forces deriving from the muscular action. These forces are complex in nature: varies over time, in intensity, in direction and in speed of application. Mechanical properties such as modulus of elasticity, yield strength, tensile strength, fatigue strength, hardness, fracture toughness are important for the material choice as already mentioned in the paragraph 1.2.1. For instance, the material of the femoral stem should have a yield strength at least of 500 MPa and tensile strength at least of 650 MPa, a minimum elongation of about 8%. Furthermore, fatigue limit should be at least 400 MPa, since the load cycles on the hip joint are about one million per year [21].

Elastic modulus should be equal to that one of the bone otherwise stress-shielding could occur (see paragraph 1.2.1).

Another issue to be considered is wear of rubbing surfaces. Joint surfaces wearing can lead to a shape changing with the consequent implant failure. Furthermore, materials debris can be generated, eliciting an inflammation in the surrounding tissues. Wear can be controlled using hard materials.

To avoid loosening of the stem and of the acetabular cup in their respective sites, frictional forces should be prevented. In fact, this would lead to early degradation and thus, to a premature implant replacement.

Finally, other three fundamental properties to be considered are density and cost, to be both minimized, and the possibility to reproduce the same properties in several prosthesis over time.

The current hip prosthesis lifetime varies between 15 and 25 years. Over the years many improvements have been made to achieve these results, but many efforts are still needed to reach even longer durations [21].

1.4.2 Common materials for femoral head and stem

First hip prostheses had the same material for both the stem and the femoral head, that is stainless steel. Later, improvements were achieved using other materials and producing the stem and the head with diverse materials. Nowadays, stainless steel is rarely utilized even if some commercial prostheses still contain AISI 316L stainless steel. Its sulfur content is very low (<0.002 wt%), therefore it is less prone to form manganese sulphides in the metal matrix that revealed to be preferential zones of corrosion initiation [31]. Anyway, this alloy is predisposed to pitting and crevice corrosion, beside its relatively low fatigue strength. It follows that its use is constantly decreasing.

As already stated, mechanical properties of the implant material should be consistent with those of bone, nevertheless, there is no material that meets all the requirements. The properties that are favored for current prostheses are biocompatibility and resistance, although the materials that satisfy these two factors have Young's moduli much greater than those of cortical bone. The metal alloys for commercial femoral stems are essentially two: cobalt-chromium alloys and titanium alloys. **Table 2** summarizes the principal mechanical properties of the metal alloys mentioned.

Table 2 Mechanical properties of the main metals alloys utilized for hip prosthetic stem.

<i>Alloy</i>	<i>Elastic Modulus [GPa]</i>	<i>Yield strength [MPa]</i>	<i>Tensile strength [MPa]</i>	<i>Fatigue limit [MPa]</i>	<i>Elongation at fracture [%]</i>	<i>Density [kg/m³]</i>
316L SS	200	689	862	383	12	7944
Ti6Al4V	115	950	1020	550	14	4420
Co28Cr6Mo	240	560	960	610	20	8290

Titanium and its alloy Ti6Al4V will be described in detail below, since at present, is the most suitable metal for hip prosthesis and for this reason is the material chosen for the experimental section in this work.

1.4.3 Introduction to Titanium

Titanium is found in nature as a compound within numerous minerals, mainly in rutile (TiO₂) an ilmenite (FeTiO₃), widely distributed on Earth's crust (major deposits of titanium minerals are found in Brazil, South Africa, India, USA, Norway and Australia). Titanium minerals have been known since the end of the 18th century, but the pure metal was first isolated only in 1910 by the metallurgist Hunter. The difficulty to obtain pure titanium lies in its high reactivity toward oxygen and nitrogen at high temperature that did not allowed its extraction from minerals using traditional steelwork technologies. In the middle of 20th century thanks to development of a process by William J. Kroll, it was possible to bring titanium to industrial scale production.

Some peculiar characteristics of titanium such as low density, high melting temperature combined with high corrosion resistance, immediately appeared interesting for many industrial applications. It was the high strength-to-weight ratio of its alloys that most of all attracted the attention of the aeronautical and aerospace sector [32].

1.4.3.1 Titanium crystal structures

Titanium is an allotropic element with a hexagonal close packed (hcp) lattice structure, called α -phase, stable below 882.5 °C, and one body-centred cubic structure (bcc), called β -phase, above 882.5 °C. In its alloys the minimum temperature at which β -phase is the only phase present is the so called β -transus. Typical α -stabilizers elements are aluminum (Al), carbon (C), oxygen (O) and nitrogen (N). Common β -stabilizing elements that forms eutectoid compounds are chromium (Cr), silicon (Si), iron (Fe) and nickel (Ni), whilst vanadium (V), molybdenum (Mo) and niobium (Nb) are isomorphic β -stabilizing elements. Finally, other elements like zirconium (Zr) and tin (Sn) do not offer a phase stabilization effect. Among all, aluminum is the most important alloying element since it enhances the alloys strength without affecting its ductility.

Depending on the microstructure present at room temperature, titanium alloys are classified into [33]:

- Alpha alloys if the percentage of β phase is less than 5%: this type of alloys cannot be heat treated but has high weldability;
- Alpha-beta alloys and near alpha alloys if the percentage of β phase ranges between 10% and 20%: these alloys respond to heat treatments and may undergo martensitic transformations;
- Beta and near beta alloys for β phase percentages above 20%: these alloys can be subjected to heat treatments but cannot undergo martensitic transformations.

The choice of heat treatment in the last two classes of alloys significantly influences the static strength and ductility beside its fracture toughness and the fatigue strength.

Alpha-beta alloys will be detailed below, with particular attention to the Ti6Al4V alloy.

1.4.3.2 Corrosion resistance

Titanium is a highly reactive metal, to the point of being more unstable than its oxide, both in the presence of air and water. It is precisely this great reactivity that

makes this material extremely resistant to corrosion, even in saltwater. In fact, this metal is protected by a surface film of oxide, 25 to 100Å thick, that forms spontaneously and quickly reforms after a damage. This phenomenon is the so-called passivation. This protective layer can be further reinforced by anodic oxidation. Over time oxide layer is reinforced and increases in thickness. Once implanted *in vivo*, the oxide layer is first hydrated, then covered with molecular layers of water and molecules such as proteins, proteoglycans, lipoproteins, glycosaminoglycans forming a dynamic interface. The final layer, in contact with mineralized tissue is made up of collagen fibers.

Direct growth of bone is possible on the surface of titanium implant, leading to an adhesive osteogenesis on a 20 nm thick proteoglycans layer. This gives a bone-implant bond resistant to traction. What has now been described is known as osseointegration. Titanium allows for a good biocompatibility since it has an excellent resistance to corrosion and a very low rate of diffusion of metal ions within the surrounding tissues, associated with an apparent absence of biological effects. Moreover, compared to other alloys used in implantology, its resistance to fatigue corrosion is higher and its elasticity modulus is closer to that of the bone. Nevertheless, some drawbacks were lately pointed out: in addition to its high cost, it exhibits poor wear behavior and long-term postoperative analyses showed the presence of bluish color in adjacent tissues due to the releasing of titanium wear debris. Furthermore, some cases of sensitization to some alloying elements such as vanadium have been described. The biocompatibility of titanium and its alloys is not always ideal due to the mechanical disruption of passivating layer due to shearing forces. Finally, the changes in surface charge can lead to variations in the conformation of absorbed proteins which, in turn, may involve a biological reaction. In fact, some proteins can be altered to the point of being recognized as antigen.

1.4.3.3 Ti6Al4V

Ti6Al4V is the most utilized titanium alloy in the world. More than 80% of its use belongs only to the aerospace industry. Another extensive application of this alloy is intended for medical prosthetics [34]. The marine, chemical and motor industries employ it as well, even if in smaller amounts. Ti6Al4V offers outstanding resistance

to medium-low temperatures but has a great specific resistance and stability also at temperatures above 883 °C, beside a good corrosion resistance. Once machined, Ti6Al4V is a very advantageous material for prosthetic implants thanks to its low Young's modulus, good tensile and compressive strength, good fatigue resistance and excellent biocompatibility (see **Table 2**).

Since titanium may undergo allotropic transformations, microstructure in α - β alloys can be considerably modified by heat treatments, thus significantly changing mechanical properties. The final microstructure is strongly influenced by processing as well. Typical microstructures that can be produced in Ti6Al4V alloy are lamellar, equiaxed and bimodal [34] as showed in **Figure 3**.

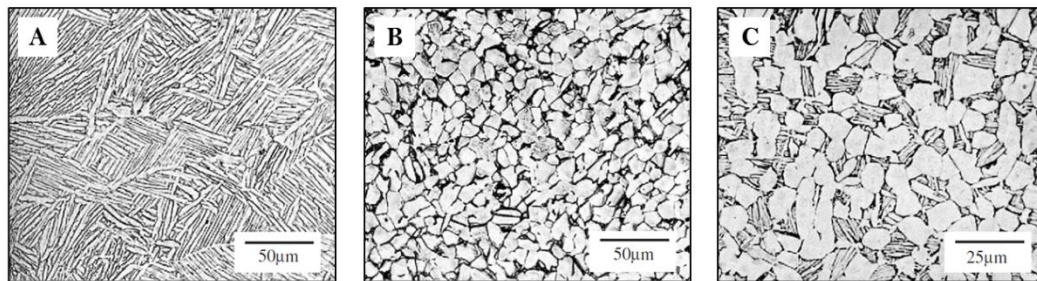


Figure 3 Typical microstructures of Ti6Al4V alloy; (A) lamellar, (B) equiaxed and (C) bimodal. Adapted from [34].

The lamellar structure can be obtained by air cooling (annealing) starting above the β transus. With this heat treatment is possible to produce the so called Widmanstätten structure: α plates, transformed by the β matrix through nucleation and growth, separated by the β phase. The size of the platelets depends on the cooling rate, the greater the rate, the finer the microstructure. Extremely fast cooling will lead to a martensitic (diffusionless) transformation. Unlike the martensitic transformation in steels, in this case the increase in hardness and strength is minor. Furthermore, in titanium alloys there are two forms of martensitic structure depending on the content of alloying elements. For reduced contents of β -stabilizing elements, the crystal lattice becomes hexagonal and the martensite is defined as α' . Whereas for high solute content, martensite has orthorhombic crystal structure and is called α'' . Annealing is normally followed by an aging treatment in order to obtain the formation of the Ti_3Al reinforcement precipitate in the α phase [33].

The bimodal microstructure (or duplex microstructure) can be obtained by solution treatment below β transus, cooling in air and a final aging treatment. This kind of structure consists of equiaxed grains of primary α phase and a fine lamellar structure of secondary α phase.

The equiaxed structure can be obtained similarly to bimodal one, the only process parameter to be modified is the rate of cooling from the temperature at which recrystallization annealing is performed. If this is sufficiently slow, there is no formation of a lamellar structure among primary α phase grains, but they tend to enlarge.

Equiaxed microstructure offers high strength and ductility despite a relatively low fracture toughness, whilst lamellar microstructure confers to the alloy a good fracture toughness despite a not remarkable strength and ductility. The duplex microstructure, being a combination of the two previous structures, provide the best trade-off between properties [34].

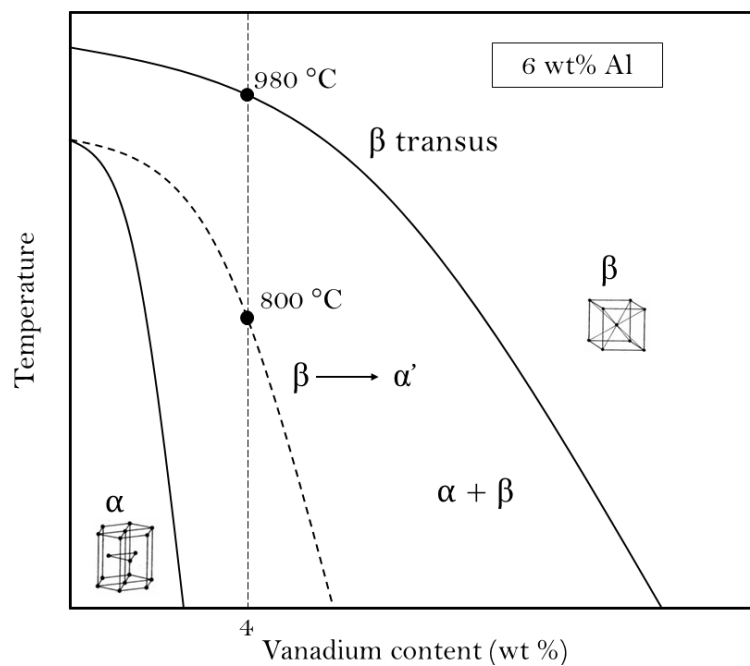


Figure 4 Ternary diagram for Ti6Al4V alloy showing the microstructure changes occurring at different temperatures.

1.5 Manufacturing technique for metal prosthesis – The EBM technology

The Electron Beam Melting (EBM) is a typology of additive manufacturing for metal components. It consists of a vacuum melting process where a bath of powders of the raw material is preheated and subsequently fused by an electron beam accelerated up to 150,000 km/s (one-half the light speed). A magnetic lens system focuses the beam, while a second magnetic field guides the electron beam to the desired spot. A variation in the current intensity and the scanning speed can induce variations of the microstructure and of the final properties. The distinct advantages of the EBM process are [35]:

- The ability to create geometric structures of complex and interconnected shape directly from the 3D CAD file;
- The component obtained has metallurgical characteristics similar to those of a quenched and tempered component, allowing to skip the heat treatment steps, with a further time and costs saving;
- The time to market of the product is reduced compared to the traditional technologies with the possibility of achieving more solutions for a given project at the same time.

Typical sectors where EBM is widely employed are aerospace and aeronautics, where high weight control and variable densities systems are required, and automotive, for frame production, allowing for weight reduction and complex shapes using high performance materials.

However, biomedical field is one of the sectors that have most benefited from this technology, allowing to obtain patient-specific components in titanium, cobalt-chrome or stainless steel for orthopaedics and to fabricate porous structures to promote the osteointegration.

1.6 Engineered surfaces

The surface is the mean by which materials interact with the external environment. Its characteristics, both chemical and physical, deeply affect the manner the material behave in particular conditions or rather its functionality [36]. This explain the reason why last decades are characterized by great investigations of surface phenomena, mainly at microscale and nanoscale. These studies allowed the development of numerous innovative fields such as electronics, optics, tribology, biomedical and so forth. The production and the control of surface features are possible thanks to advanced instruments and technologies exploiting mechanical, chemical or physical methods [36]. The result is a microtextured surface, characterized by a regular pattern of micro-holes or micro-asperities with a precise shape and dimension [37]. At present, surface texturing is a topic of great interest in the research field, but more versatile, simple and cheap manufacturing technologies are needed to bring the production on a large scale.

1.6.1 Applications

As already stated, studies on engineered surfaces allowed the development of numerous innovative fields having a wide number of applications. In literature it is possible to find lot of examples of their industrial and laboratory applications. Below, some of the most fascinating fields of applications are reported.

Energy field

Structured surfaces have been widely studied for heat transfer phenomena in diverse industrial fields such as electronics, aerospace and power stations. In fact, the surface's microstructure allows an increase of contact area between solid and its coolant influencing the heat transfer. Mainly spray and boiling mechanisms have been considered by researchers. Spray cooling is a multiphase convective process capable of high heat fluxes dissipation with low coolant mass fluxes. The factors that affect the spray heat transfer are primarily the volumetric flux of the spray and secondly the fluid temperature, the conditions of the surrounding environment and the surface irregularity. Higher the surface roughness, higher the heat transfer coefficient for liquid-atomized sprays, whilst gas-atomized sprays are more

effective in cooling smooth surfaces. In general, it can be stated that irregular surfaces are more efficient in heat transfer compared to plane surfaces but a direct proportionality to the contact area is not always present. These results point out that mechanisms at the basis of spray cooling are complex and further investigations are needed to completely understand the controlling phenomena.

In several industrial and domestic applications boiling has a great role. It consists of the vaporization of a liquid when it reaches its boiling point. In the nucleate boiling phenomenon, small vapor bubbles form at discrete point, called nucleation sites, of a heating surface. Homogeneous nucleation occurs within the boiling liquid, whereas heterogeneous nucleation happens at the solid–liquid interface. The latter has been extensively investigated due to its industrial relevance. Features that influence this phenomenon are process parameters such as temperature and pressure beside surface topography, solid and liquid properties. In particular, the density and the design of nucleation sites are key factors to understand and control boiling. In the recent years many researchers developed several techniques to improve the heat transfer creating artificial nucleation sites, i.e. surface cavities and reentrants. These engineered surfaces are widely utilized in many industrial applications such as water chillers.

Microfluidics

Microfluidics is the science dealing with the behavior and control of fluids through micro channels. Therefore, this science requires precise modification of surfaces to manipulate the fluids flux and many engineered surfaces for this purpose are proposed in literature. An example of application in this field is the possibility to cause a liquid flow using only electrostatic effects, as reported in [38]. To do this, a special pattern, having hydrophilic and hydrophobic regions, was printed on the substrate to confine the liquid droplets that move under localized electrostatic fields.

Optics

Another important field where structured surfaces play an important role is optics. Recent developments in micro-optics lead to a shift from refractive to diffractive optical elements to fulfill increasingly tendency towards miniaturization in many industries such as computing, aerospace, automotive, electronics. Generally,

diffractive elements are manufactured with precision cutting processes such as diamond turning and milling or with lithography. Laser technique is reported in some studies as well [39].

Bioengineering

In the last thirty years tissue engineering and biochips became attractive therapeutic means. They are the result of interdisciplinary fields such as microbiology and engineering where surface properties play an essential role. For instance, patterned surfaces seem to be a fundamental mean through which communicate with cells to help their adhesion and growth [40].

Cleaning

Surface texturing can be exploited to produce water repellent surfaces taking inspiration from lotus leaf surface structure. This feature is already utilized in some commercial products such as repellent shower glass or repellent clothing.

Manufacturing

Structured surfaces have been taken into consideration also to improve the efficiency and productivity of manufacturing processes. For instance, some studies have stated that it is possible to ameliorate the surface finishing while polishing by shaping the abrasive grains of belts into specific geometries. Moreover, heat generation is reduced extending belt's lifetime [41].

1.7 Engineered surfaces technologies

Many industries and research groups developed various methods to modify surface topography on a microscopic scale [42]

This paragraph will describe some of these methods, classifying them into four groups, based on physical principles: adding material, removing material, moving material, self-forming [36].

1.7.1 Adding material technologies

In adding material technologies, the surface pattern is obtained through the addition of matter on the surface generating tiny relief zones.

The methods to obtain this surface texturing can be both physical or chemical. In the first case the deposition is promoted or inhibited by a previous chemical or physical local modification of specific surface areas to create the desired pattern. For instance, to shield the stream in physical vapor deposition (PVD) a masking can be utilized. Chemical processes utilize special inks, deposited on the surface to favor or not some chemical reaction for the creation of the surface texture.

Alternatively, inks can be placed on the substrate to create directly the wanted feature, that is inkjet printing. Materials that can be printed are metals, ceramics, structural and conductive polymers, sol-gel materials and organic transistors [36]. For this technique the best resolution that can be achieved is about 15 μm . Another technique for material deposition, with resolution better than 100 nm, is the focused ion beam technique (FIB) nevertheless, this method is particularly slow. Thermoset polymers can also be utilized as coatings starting from a liquid resin and arranging the material into the desired pattern while curing.

Surface texture on a nano scale can be obtained by spin coating. In this technique, a colloidal solution of nanoparticles is deposited onto the surface. Thanks to the wide assortment of the existing nanoparticles in the market, this process is highly flexible. In fact, various nanotextures can differ from each other in terms of density, size and material.

1.7.2 Removing material technologies

In removing material technologies, the surface topography is generated by the removal of material from the surface, forming tiny depressions. The processes owing to this group are high temperature processes, chemical etching processes and mechanical processes. Typical texturing methods of this class are described below.

1.7.2.1 Chemical texturing

This kind of texturing utilizes chemical reagents to locally and selectively remove material from a substrate. The surface to be textured is immersed in the etchant after masking the areas to protect from the chemical attack.

The reagent removes the material by electrochemical cell action at microscopic level, leading to a local corrosion or dissolution, thus the mechanical properties of textured regions are not changed. The method utilized to mask the surface highly influence the features resolution, while the process duration is mainly linked to the speed of the etching process.

For instance, in photochemical etching (PCE) the surface etching depends on different conditions such as the temperature of the corroding bath, local gradients of the etchant, the reagent diffusion rate and the distribution of the shielding masks. In some particular methods there is no need for masking prior etching (maskless electrochemical texturing). An example could be self-assembling particles or droplets in specific patterns, followed by etching. These methods significantly decrease process time and cost, exploiting hydrophobic and hydrophilic zones of a substrate.

1.7.2.2 Mechanical texturing

In this case mechanical action is utilized to remove the surface material from selected areas. The conventional way to do so is by means of a cutter. The surface topography is thus obtained by conventional finishing processes such as grinding, honing, turning or polishing, or by means of novel processes such as ultrasonic machining. Other methods can exploit the abrasion action of some particles to mechanically remove the material.

1.7.3 Moving material technologies

Moving material technology can be both chemical or mechanical. The surface topography is obtained by plastic deformation and redistribution of the surface material. In some case it can lead to a strain hardening of the surface thus in an increase of surface hardness. Usually, this type of process is utilized for materials

that show a ductile surface such as high ductility metals or thermoplastic polymers. A method belonging to this class is shot blasting (SB). A high-speed shot of hard microparticles impacts the surface causing its roughening by plastic deformation. The main drawback of this technique is the low control on the surface topography since velocity, shape, size and hardness of the shot cannot be precisely predicted. The final texture will thus be random. In the case of thermoplastic polymeric material texturing, the surface should be previously heated up till plasticization for an ease deformation. It follows that hard tools are not necessary for this process, reducing costs but allowing for a well resolved surface structure. On the contrary, to emboss harder materials such as ceramics, microstructured diamond tools are typically utilized.

For plastically deforming the surfaces of metals, it is possible to use vibrorolling. In this method the tool is composed of a highly hardened ball or a round diamond tip that hit the surface. The result is a fine-scale textured surface with regular microasperities.

As previously stated, also chemical reactions can be used to deform the material surface. Some studies report a nano-texturing exploiting molecular migration stimulated by a laser beam. Furthermore, also the contraction of polymers that are photocurable can be exploited for surface texturing; it is simply necessary to place a metal shield between the UV source and the liquid resin.

1.7.4 Self-forming technologies

Self-forming by wear technologies exploit the normal surfaces wear to create the required texturization. It is known that load bearing surfaces are subjected to high stresses, particularly shear ones. These stresses modify surface topography wearing out the asperities that, initially, carry most of the applied load. To exploit favorably this effect, some researchers argue that is possible to manipulate the surface creating some regions resistant to wear, with better mechanical properties, in order to vary the wear rate in the substrate, contributing to the creation of the desired topography. To generate the mechanical proper gradients, it is simply possible to use traditional metallurgical treatments.

1.8 Advances in materials functionalization

In the biomedical field, mainly in the production of long term implants, there is an increasing need to realize components characterized by a long life to avoid painful and costly secondary surgery for revision [43], [44]. Moreover, the increased longevity and a growth of younger, more active patients, push the research towards increasingly performing prosthesis [45].

In this framework, depending on the particular prosthetic component, the processes utilized to manufacture it should allow a significant improvement of characteristics such as tribo-corrosion, fatigue and wear resistance, stress-corrosion cracking resistance [46].

The usual process chain for producing metallic prosthetic components involves plastic deformation followed by machining operations and finishing operations. The latter are designed to give the component the necessary surface integrity. Finishing operations can include machining operations such as grinding, lapping, superfinishing and/or surface quality modification processes that do not involve geometric variation such as coating, heat treatments, etc. It can be seen that the number of manufacturing processes steps that are necessary to produce the component is particularly high. Moreover, finishing operations are not always able to ensure the surface integrity such as to meet the requirements in service life to avoid revision operations. In the last years, some research groups have developed possible solutions to increase the lifetime of prosthetic components based on the surface functionalization. An example of application is related to the coupling surfaces of hip prosthesis, surfaces that should be characterized by a high wear resistance to avoid periprosthetic osteolysis and a premature revision. In particular, this functionalization can be achieved by the creation of a patterned micro-texture on the components' surface. The studies demonstrate that an array of concave micro dimples enhances the load-carrying capacity and the lubricant film thickness allowing for friction and wear reduction.

Ito et al. [47] manufactured circular dimples of 0.5 mm in diameter and 0.1 mm deep, with a 1.2 mm pitch on a CoCr femoral head. They observed a 17% friction reduction and a 36% reduction in polyethylene wear. They hypothesized that this may be the result of the abrasive wear particles being trapped in the dimples and

lubricant being accumulated and subsequently dispensed from the dimples during lubricant starvation conditions.

Sawano et al. [48] used a waterjet to machine 0.25 μm to 4.4 μm deep channels, spaced 10 μm apart from each other and running perpendicular to the direction of articulation, into a CoCrMo plate. A limited reduction in polyethylene wear was measured in a pin-on-disc experiment, which was attributed to the channels trapping wear particles. Laser surface texturing was used by [49], to generate different patterned micro texture on the surface of a CoCrMo plate. It was demonstrated that, thanks to the increasing of the lubricant thickness the coefficient of friction was reduced.

Nevertheless, all the cited studies make use of further complex and costly manufacturing processes, prolonging the process chain and thus time and expenses. Recently, at the University of Padua, machining processes that have shown a considerable increase in the lifetime of titanium alloy prosthetic components and of magnesium alloy for bioabsorbable implants have been developed [50], [51]. The aim of this line of research is to introduce new machining processes, eventually assisted by low temperature coolant, modifying the surface integrity of prosthetic components to improve its service life performances. The innovative machining processes utilized in the just mentioned works are Ultrasonic Vibration-assisted Turning (UVT) and Large Strain Extrusion Machining (LSEM). The first process involves using a tool that vibrates at ultrasonic frequency to create surface textures of controlled geometry, while the second process involves a combined machining and extrusion process. In the manufacturing scenario, UVT shown to be a potential way to texturing surfaces during machining without adding any addition machining step to the manufacturing chain. Moreover, the novelty of these studies lies in the fact that just few researchers have experimentally attempted to evaluate tribological performances of UVT-ed workpieces and none of them applied this method for biomedical purposes.

In [52], the effect of machining process parameters and vibration mode on the tribological properties of steel and its counterpart is investigated. Results show that textured surfaces are characterized by lower coefficient of friction and wear rate. Xing et al. [53] examined tribological properties of aluminium alloy surfaces resulted from ultrasonic vibration assisted milling method compared to

conventional surfaces, showing a 20% decrease in friction and 140% increase in oil retention.

In this study, for the first time, UVT is presented as an innovative solution to face overcome infections issues in total hip replacements, which often brings to a premature postoperative revision in total hip replacements.

1.9 Introduction to Ultrasonic Vibration Turning

One promising and still-to-explore machining technology to engineer surfaces is the UVT. The benefits of controlled ultrasonic vibrations in cutting was first investigated in the middle of twentieth century [54]. In this technique the high frequency alternative motion superimposed on the cutting tool has interesting consequences both on the surface texture and on the cutting process itself. In fact, with UVT it is possible to machine even brittle materials such as glass and ceramics or difficult to machine materials such as titanium or nickel-based alloys, extending tool life, thanks to a decrease in cutting temperature and in cutting forces [55], [56]. This kind of machining operation allows to improve surface finish resulting in a fine precision turning of texturized surfaces. Improvement in mechanical and optical properties can also be reached [56]. The surface pattern given by the UVT encountered high interest in the tribological systems, where surfaces play a key role. In fact, the material removal in this type of machining creates micro-dimples that can act as reservoir of lubricant or as micro cavities able to entrap cutting debris, avoiding abrasive wear [36]. All these features contribute to an improvement of wear resistance.

The possibility to machine titanium alloys linked to the presence of dimples for fluid storage lead us to the idea of exploiting UVT to overcome infections issues in total hip replacements. A flare of the body's inflammatory response often brings to a premature postoperative revision in total hip replacements. The surface valleys could be possible sites to store drugs in order to create functionalized surfaces able to act against infection onset *in situ*.

Below, a description of the UVT functioning is presented.

1.9.1 Summary of different type of UVT

In UVT the conventional cutting process is combined with high frequency and low amplitude vibration to reach the already stated improvements. Frequencies range from few kilohertz to 40 kHz with a predominance of systems working around 20 kHz, whereas amplitudes vary within some units of micrometers up to 100 μm [56]. Vibration assisted machining can be classified in two main groups depending on the frequency vibration [56], [57]:

- Resonant systems if a piezoelectric transducer generates vibrations matching with the natural frequency of a sonotrode to which it is connected;
- Non-resonant systems in which sinusoidal voltage signals cause the transducer to vibrate at a frequency lower to the system natural one.

Resonant systems offer only discrete frequencies, moreover the servo produces displacement amplitudes less than 6 μm . On the contrary, with non-resonant servos, operating frequencies and amplitudes ranges are more than ten times higher than in resonant systems. Nevertheless, the greater control and displacement lead to a lower tool speed and bigger power requirements.

Depending on the motion of the vibrating cutting tool, these two main classes can be further subdivided into [56]:

- one-dimensional vibration assisted machining when the system works with a linear motion lying on a parallel plane respect to the workpiece substrate, in line with the cutting force.
- two-dimensional vibration assisted machining when the system works with an elliptical motion having the major ellipse axis in line with the cutting force and the minor one in line with the thrust force. In this case the vibration amplitude in the two directions can or not match.

In **Figure 5** are schematically represented the different types of UVT systems.

Type	Vibration in cutting direction	Vibration in normal direction	Vibration in cutting/normal direction	Elliptical vibration
Tool tip trajectory				
Tool tip motion	1D systems			2D system

Figure 5 Different types of vibration cutting systems. Adapted from [55].

1.9.2 Servo Designs

The progress in the tool servos construction reflects on the development of vibration cutting systems. In 1D vibration assisted machining the simplest servo is utilized. The first researches made on vibration cutting operated with this kind of system. In **Figure 6** is showed the design of 1D servo developed at Fraunhofer institute, similar to the first servos design, utilized to study ultrasonic assisted diamond turning of steel and glass [58].

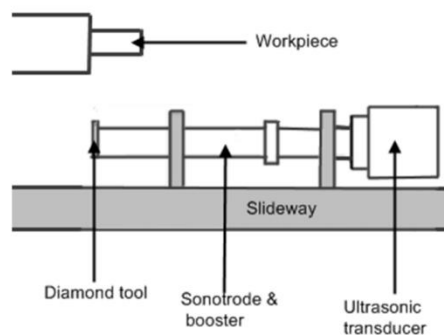


Figure 6 Servo design from Fraunhofer IPT, Germany. Adapted from [58].

In this servo, a piezoelectric transducer generates longitudinal vibrations with a frequency 40 kHz. The transducer is then connected to an amplification horn through a sonotrode. The ultrasonic energy input sets up a longitudinal resonance in the booster thanks to the specific design of the sonotrode, a non-amplifying resonator, causing an increase in the vibration amplitude. This arrangement allows for a $\pm 5 \mu\text{m}$ sinusoidal displacement of the tool [58].

A research group in Germany (University of Bremen), discovered that decentralizing the tool tip, an elliptical path of the tool itself was produced [59]. A piezoelectric converter was coupled with an ultrasonic generator at 40 kHz making the tool vibrating. An amplitude of $6\mu\text{m}$ was generated vertically through a sonotrode-booster complex. Finally, a bending resonance was obtained placing the tool tip off the sonotrode axis. The sum of the vertical and horizontal displacements resulted in an elliptical path of the tool tip motion. The motion path can be slightly varied using a counterweight. The system described is showed in **Figure 7**.

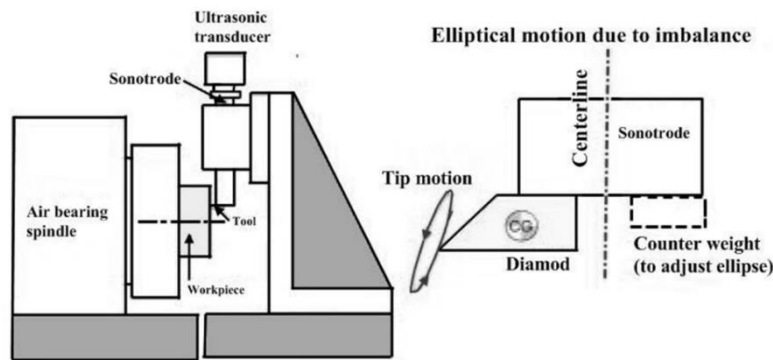


Figure 7 Servo design from Bremen University, Germany. Adapted from [59].

As previously stated, servos can be resonant or non-resonant. The Pusan University designed the latter one as illustrated in **Figure 8** utilizing two piezo actuators oriented at right angle to each other parallel to the upfeed and vertical directions [60]. To hinder the crosstalk between the two direction, the flexure has an internal cross-shaped hole. The tool is placed on the opposite side of the actuators (see **Figure 8**). The servo operates at 1 kHz with ellipse axes of $5\mu\text{m}$ maximum.

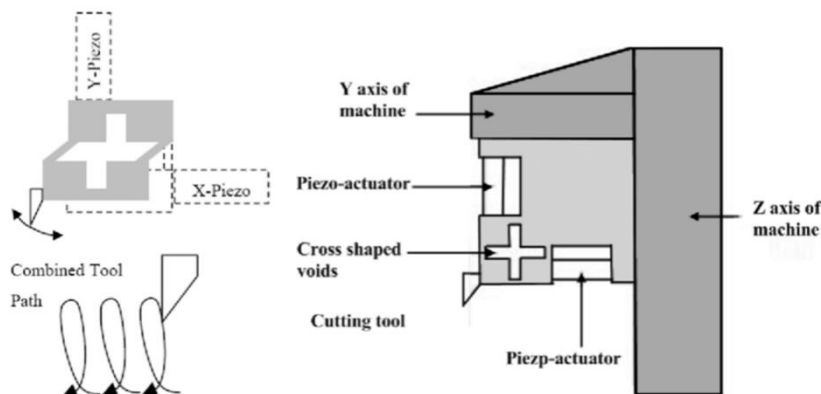


Figure 8 Servo design from Pusan University, South Korea.

In **Figure 9** is shown a resonant 2D servo implemented by Moriwaki and Shamoto [61]. A beam structure support two piezo actuators that are triggered in opposed pairs causing bending in the upfeed and vertical directions. At the end of the same beam the tool tip is placed. The union of the two bending vibrations at angles of 90° make the diamond tool move in an elliptical track. This system can operate at frequencies in the range 20–40 kHz with typical operating toolpaths of $3\ \mu\text{m}$. Later, the authors added a third vibration in the feed direction, creating a 3D version of this tool.

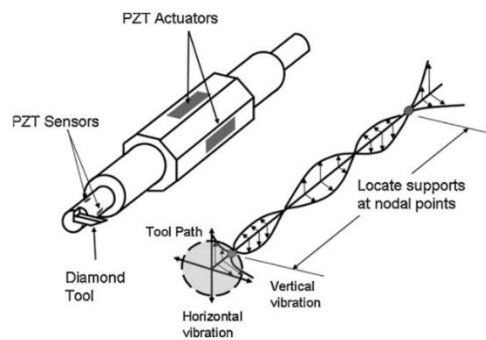


Figure 9 Resonant 2D servo actuators implemented by Moriwaki and Sakamoto. Adapted from [61].

1.9.3 Kinematics of vibration-assisted machining

Figure 10 displays the 1D UVT system utilized in this work and its coordinate system. The X-axis is normal to the workpiece surface and lies along the direction of the depth of cut (DOC), as well as the vibration direction. The Y-axis is in the primary cutting direction that is the upfeed direction. Finally, the Z-axis coincides with the feed direction.

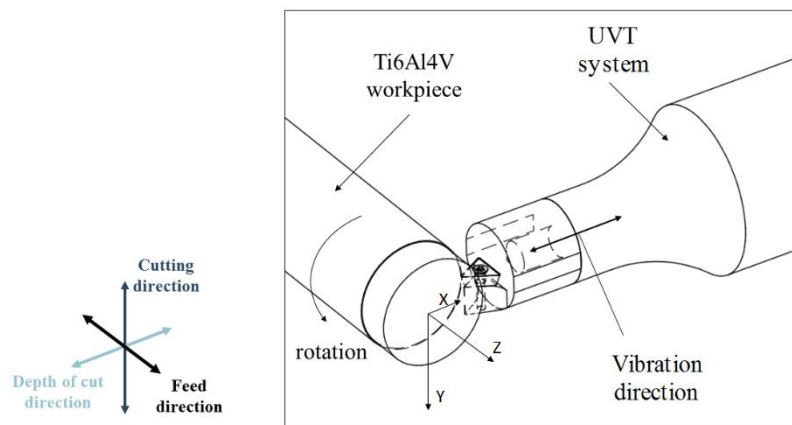


Figure 10 Coordinate system of UVT arrangement utilized in this work.

1.9.4 One-dimensional vibration-assisted machining

To understand the kinematics at the base of 1D UVT, an idealized cycle of a general vibration assisted machining is taken into consideration. The Figure below shows the scheme of a cutting cycle (the coordinate system refers to that one of the previous **Figure 11**).

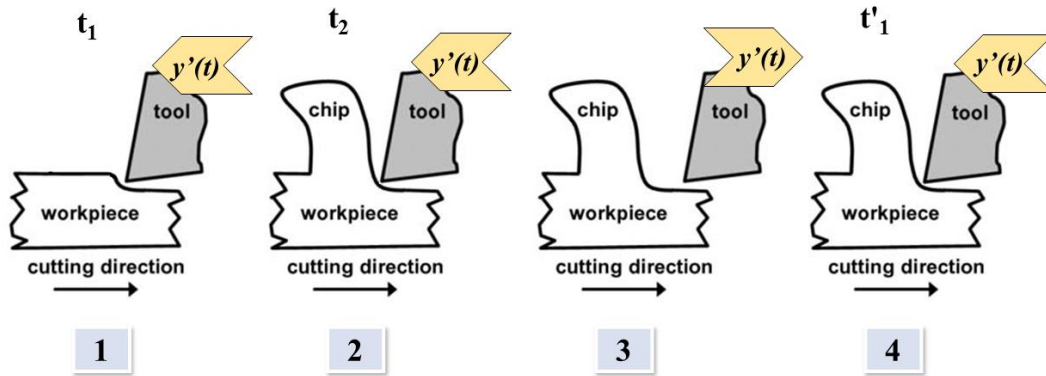


Figure 11 1D vibration-assisted machining kinematics.

The tool vibrates harmonically in a linear trajectory, along the cutting direction in Y axis. Once fixed the vibration frequency f , it is possible to outline a velocity below which the tool rake face intermittently loses contact (or, alternatively, above which never loses contact) with the uncut material of the surface, that is the critical cutting velocity [56]. The tooltip displacement as a function of time can be described by the following equation:

$$y(t) = A \sin(\omega t) + Vt \quad (1)$$

Where A is the vibration amplitude, V is the cutting velocity of the workpiece and ω the angular frequency, related to the frequency of vibration f by $\omega = 2\pi f$. To get the tool velocity, the equation describing the position is derived as follow:

$$y'(t) = \omega A \cos(\omega t) + V \quad (2)$$

In the first frame of **Figure 11**, at time t_1 , the rake face of the tool just came into contact with the virgin material and is beginning to cut ($y'(t) > 0$). In the second frame, the tool is at the end of its vibration trajectory ($y'(t) = 0$) and is about to

change the direction of motion. The time the tool loses contact with the workpiece is indicated as t_2 . In the third frame, the tool moves away from the workpiece surface, having the velocity direction opposite to that of the previous frames. In the last frame, the tool advances ($y'(t) > 0$), coming into contact with the material and another cutting sequence begin. The entire cycle lasts for a time that is defined as T , equivalent to $1/f$ and the cutting time is equal to $t_2 - t_1$.

From equation (2) it is possible to obtain the formulation of the formerly defined critical cutting velocity V_{crit} :

$$V_{crit} = 2\pi f A \quad (3)$$

Intermittent disruption of cutting is verified, at a given frequency f , if $V < V_{crit}$.

If the opposite verifies ($V \geq V_{crit}$), then the tool continuously cuts the material while a harmonic variation of the relative velocity between the tool and workpiece occurs. Intermittent cutting is usually preferred since in this case the vibration assisted machining processes shows its advantages such as enhanced surface finish, prolonged lifetime of the tool etc.

The increment in the cutting direction, d_{cutt} that coincide with the distance, expressed in millimeters, between two following gaps on the surface texture can be calculated as:

$$d_{cutt} = \frac{V}{60f} \quad (4)$$

where the cutting velocity and the frequency are respectively expressed in m/min and Hz.

Another parameter to characterize the vibration assisted machining cycle is the Horizontal Speed Ratio HSR, that is the ratio between the workpiece velocity and the tool speed:

$$HSR = \frac{V}{2\pi f A} \quad (5)$$

For non-interrupted machining the HSR value is value is greater or equal to one ($HSR \geq 1$).

The fraction of contact time in one vibration cycle is the so-called duty cycle. For 1D vibration assisted machining the duty cycle DC_1 is defined as:

$$DC_1 = \frac{t_2 - t_1}{T} = f(t_2 - t_1) \quad (6)$$

All the variables that appear in the equation were formerly defined. The higher the duty cycle value, the higher the cutting time in each cycle. DC is equal to one ($DC = 1$) for non-interrupted and conventional machining. The graph below (**Figure 12**) displays the duty cycle as a function of HSR in a one-dimension system.

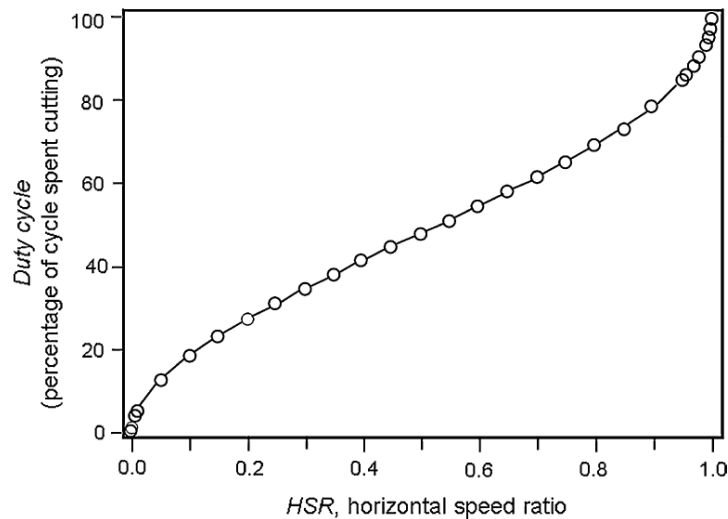


Figure 12 Representation of duty cycle as a function of horizontal speed ratio of a 1D vibration assisted machining [56].

In the interests of providing fuller information, the kinematics of a 2D system will be briefly described in the following paragraph.

1.9.5 Two-dimensional vibration-assisted machining

Two-dimensional vibration assisted machining combines a vertical and a horizontal harmonic motion. The tooltip trajectory becomes elliptical, leading to a different surface topography respect to one-dimensional systems. **Figure 13** shows the toolpath during a 2D cutting process.

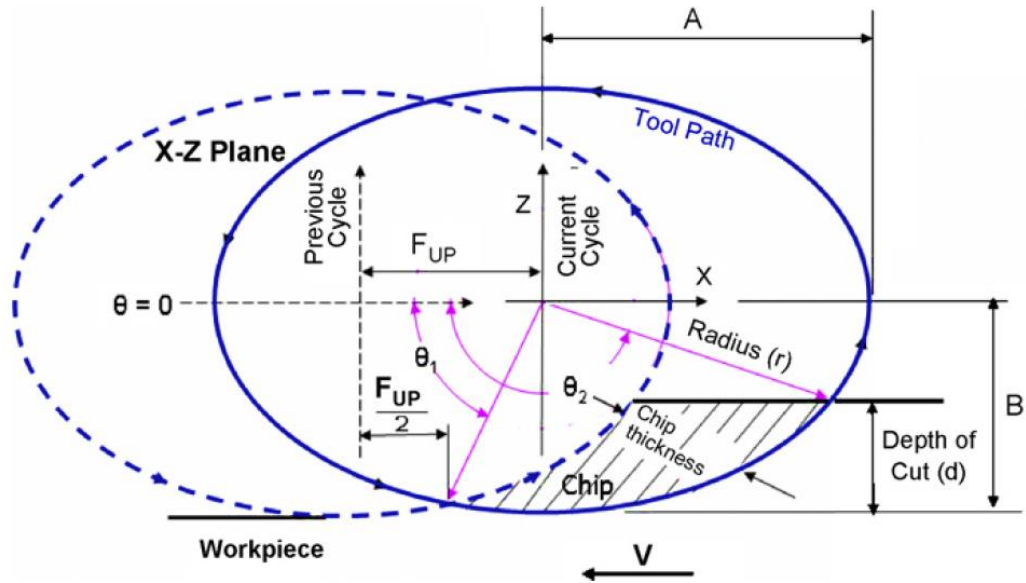


Figure 13 2D vibration-assisted machining kinematics, displaying the typical elliptical toolpath [56].

This approximative scheme occurs when the workpiece displacement in the cutting direction is lower than the horizontal vibration amplitude A .

The vertical $z(t)$ and the horizontal $x(t)$ tooltip displacement as a function of time are respectively described as:

$$x(t) = -A \cos(\omega t) + Vt \quad (7)$$

$$z(t) = -B \sin(\omega t) \quad (8)$$

where B is the amplitude of vertical vibration. In particular, A and B are respectively, the major and minor semi-axes of the elliptic path. The other variables were already defined in the previous paragraph.

The tooltip velocity is can be obtained from the of equations 7 and 8:

$$x'(t) = \omega A \sin(\omega t) + V \quad (9)$$

$$z'(t) = -\omega B \cos(\omega t) \quad (10)$$

It is important to state that **Figure 13** displays an angular position θ equal to ωt and that the equations from (7) to (10) refer to $\theta = 0$.

To know the instantaneous direction $\chi(t)$ of the tool motion, the following equation should be utilized:

$$\chi(t) = \arctan\left(\frac{-\omega B \cos(\omega t)}{\omega A \sin(\omega t) + V}\right) \quad (11)$$

While, for the instantaneous rake face angle $\gamma(t)$ and clearance angle $\alpha(t)$:

$$\gamma(t) = \gamma_0 + \chi(t) \quad (12)$$

$$\alpha(t) = \alpha_0 - \chi(t) \quad (13)$$

where γ_0 and α_0 are, respectively, the tool rake and clearance angle.

The formulations for critical cutting velocity V_{cutt} , increment in the cutting direction d_{cutt} and horizontal speed ratio HSR are the same reported for one-dimensional machining in the previous paragraph (respectively the equations (3), (4) and (5)).

The duty cycle in 2D vibrational-assisted machining is the percentage of the elliptical trajectory in which the tool is into contact with the workpiece [56] and can be written as:

$$\text{DC}_2 = \frac{\text{arc}(\theta_2 - \theta_1)}{2\pi\sqrt{(A^2 + B^2)}/2} \quad (14)$$

The numerator and the denominator are respectively the contact arc length and the perimeter of the ellipse. To determine the angular position of tool entry θ_1 , the following parameters should be known: HSR, A and B . While the parameters to calculate the exit angular position θ_2 are the depth of cut d , A and B .

At a given HSR, the maximum duty cycle is reached when $d/B \geq 1$, $\theta_2 = \pi$ so $d/B = 1$. In a two-dimensional vibration assisted machining the maximum value for the DC is 0.5 when d_{cutt} is sufficiently high to avoid the overlapping of two consecutive surface dimples and $\text{DOC} \geq B$.

The following graph (**Figure 14**) displays the duty cycle as a function of HSR and d/B in a two-dimension system at given A and B values (reported on the diagram).

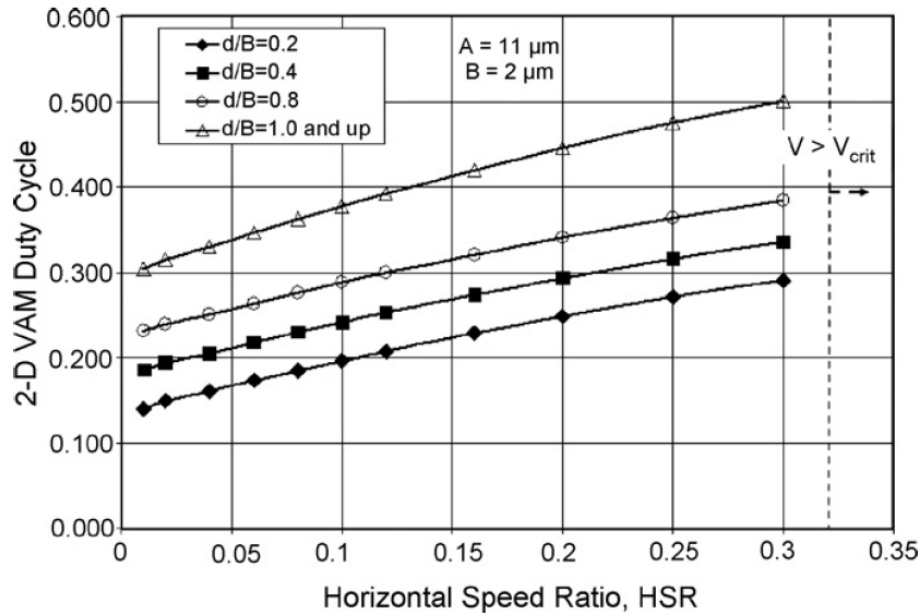


Figure 14 Representation of a duty cycle as a function of horizontal speed ratio and of the ratio between the depth of cut d and the major semi-axis of the elliptical toolpath of a 2D vibration assisted machining [56].

As already stated, in this work, the system adopted is the 1D UVT, with the cutting tool vibrating along the radial direction, perpendicular to the feed one. With this configuration it is possible to obtain micro textured surfaces in which the distance between two following gaps d_{cut} can be calculated using equation (4). In **Figure 15** is shown the UVT system designed by Di Iorio [51] at University of Padua, which was utilized for the experimental section of this work.

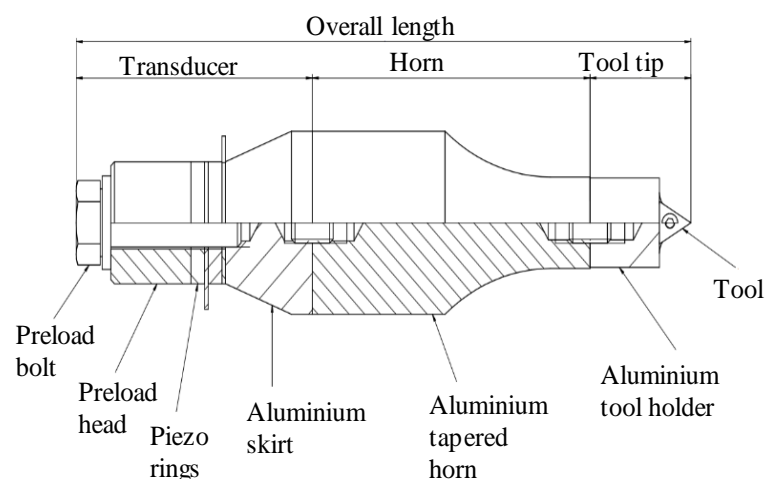


Figure 15 Servo design implemented by Di Iorio [51], University of Padua.

To assess that the presence of micro-dimples on our UVTed titanium surfaces does not alter the wear magnitude, compared to the current configuration adopted in

implants (polished smooth surfaces), tribological test were performed. The following paragraph explain the importance of this kind of testing.

1.10 Tribology

Tribology is the science that studies friction, lubrication and wear of contact surfaces in relative motion. The word derives from the composition of two Greek terms *tribos* (= rubbing) and *logos* (= study). Bhushan [62] reported that this term was first utilized by Jost in his revolutionary report.

Since tribology includes three different topics, as already stated, is thus a complex interdisciplinary subject. Generally, friction is considered a branch of physics and mechanical engineering, while wear is principally related to metal material science and lubrication is a chemistry sector. Tribology is thus a complex interdisciplinary subject.

1.10.1 History and beginnings

Tribology deals with problems affecting the community both from an economic and safety point of view. Technical equipment of a range of applications, going from the aircrafts to medical implants, undergoes wear problems, compromising its reliability and safeness, calling for a need of maintenance and special precautions. Since the Paleolithic, the man tried to solve problems related to tribology [63]. Over the years there has been an increasing awareness of the physics of friction and wear. Among all the early researchers it is worth to cite Leonardo da Vinci (late 1400s) who first approached methodically the friction phenomena, Amontons (late 1600s) and Coulomb (late 1700s) who derived the first laws. A great push to studies on tribology was given by the industrial revolution. Nevertheless, only at the end of the 19th century a scientific understanding of lubricated bearing operations was attained. For what concerns hydrodynamic lubrication studies, Reynolds (late 1800s) gave an important contribution. Finally, wear studies have been poor until the middle of the 20th century. The huge industrial development started at the beginning of the 20th century allows for a great understanding and knowledge of all the tribology sectors [63].

1.10.2 Friction

Kinetic friction is the force that resists the relative motion of one body over another. The resistance is due to the intrinsic roughness that characterizes any type of surface. The real contact area between two surfaces is that between microscopic bumps which exert adhesion forces. A certain shearing force must be exercised to put the two surfaces in relative motion since the micro-welding should first be destroyed.

The bases of kinetic friction are described by three simple laws:

- friction is directly proportional to the applied load (Amontons' first law)
- friction is independent of the apparent contact area, but is dependent to the real contact area (Amontons' second law)
- friction is independent of the sliding velocity (Coulomb's law of friction)

The Coulomb model is utilized to describe the first law mentioned above and it is governed by the following equation:

$$\mu = F/N \tag{15}$$

where μ is the coefficient of friction, frequently designated as COF, F the friction force parallel to the surface, directed in the opposite direction of the motion and N the normal load exerted between the surfaces.

Static friction is the force between two surfaces not moving with respect to each other. The force to exceed static friction is always higher than the force to exceed kinetic friction. It follows that the coefficient of static friction is greater than the kinetic friction one.

1.10.3 Wear

Wear can be defined as the origin of material loss on a microscopic scale [64]. The progressive removal of material from a solid surface can be mainly ascribed to the mechanical action exerted by another body.

1.10.3.1 Classification of wear mechanisms

Since wear can be caused by a variety of factors, it is important to make a distinction. To do so, changes in surface topography and the condition at which the wear occurred are the key factors to take into consideration. A first rough classification of wear consists in differentiate single phase from multiple phase wear [63]. In the first case a solid, a liquid or a gas, in relative motion to a body, leads to material removal, thus to wearing of the latter. In the second case, wear is due to the presence of a third body in a carrier, such as particles or asperities, sliding against a body. There is still a lack of categorization describing the state of stress and the chemical conditions on materials undergoing wear mechanisms. Nevertheless, a common classification divides wear typologies into: adhesive, abrasive, fatigue, fretting, erosive and corrosive [65].

Adhesive wear occurs when two sliding surfaces are subjected to frictional contact leading to the detachment and the following attachment of wear fragments from a surface to another. This material transfer is due to plastic deformation of tiny debris between the two sliding surfaces, leading to increased surface roughness and surface irregularities. This type of wear can be suppressed using a good lubricant.

Abrasive wear takes place when hard particles or hard asperities slide against and along a solid surface, causing a progressive removal of material or the formation of surface grooves. Abrasion occurs since the surface to be scraped is softer than the rough constituent, thus it can be avoided hardening the solid surface or eliminating the hard body.

Fatigue wear refers to a gradual and localized structural damage caused by a cycling loading throughout friction. It takes place when the material fatigue strength is lower than the applied load. The severe plastic deformation caused by fatigue wear give rise to the onset and propagation of subsurface cracks, and the subsequent failure of the component. It usually starts from micro pitting areas on the surface leading to spalling.

Fretting wear can be seen as a typology of fatigue wear and it is caused when small amplitude oscillatory movements occur between two sliding surfaces. The friction forces produce switching compression-tension stresses, leading to surface fatigue.

Erosive wear is caused by particles impact on the surface of a component. The repetitive short and fast sliding motion of those fragments leads to deformations and cutting action, causing a gradual material removal. One of the most important factors influencing the erosion rate is the impingement angle. Ductile materials are mostly affected if impingement angle is 30° , while materials that are not ductile are more susceptible if the angle is 90° .

Corrosive wear occurs when worn material reacts chemically with the corroding environment. The most common corrosion products are oxides that split apart, due to their different shear strength from that of the metal substrate. A synergistic action of tribological stresses and corrosion is known as tribocorrosion.

1.10.4 Lubrication

To reduce wear and friction, lubrication is crucial. A lubricant is a substance placed between two surfaces in relative motion that increases their distance, diminishing the detrimental effect of surface asperities and abrasive debris. Moreover, a lubricant has other important functions. It can be exploited to cool down the heat produced at the level of mating surfaces and to limit corrosion. In fact, lubricant serves as a preservative during machinery idle while, during machinery using, it coats the lubricated components forming a protective layer that hinder corrosion onset. For this scope, also lubricant chemical composition has to be taken into consideration.

Lubricant can also be used as hydraulic fluid in hydraulic transmission systems, as cleanser to remove contaminants, as electrical insulator in electrical devices and as shock-damper in shock absorbers.

1.10.4.1 Lubrication regimes

There are three types of lubrication regimes: full film, boundary and mixed. The classification depends on the ratio between the fluid film thickness h and the surface roughness R_a [66].

Full film lubrication when $h \gg R_a$.

In this type of regime, a fluid film fully separates the sliding surfaces. The pressure in the lubricant layer is higher than the bearing load avoiding the contact between the surfaces. It verifies when the system is characterized by high speeds and/or low unit loads. A further subdivision of full film lubrication depends on the type of lubricant pressure supply. If it is external the lubrication is hydrostatic, while if the pressure is generated by the system kinematic and design, the lubrication is hydrodynamic. The latter typology is highly influenced by the lubricant viscosity and a direct proportionality links friction to viscosity.

Boundary lubrication when $h < R_a$.

If bearing surface micro asperities are constantly into contact the lubrication regime is the boundary one. It is characterized by a high coefficient of friction, thus by high energy loss and heat generation, leading to an increase in wearing, to localized pressure peaks and to an increased possibility of seizure. Boundary lubrication causes severe bearings failures and commonly occurs during the engine start and shutdown when the speed friction is low, the loads are high, or the lubricant has low viscosity. Some oily lubricants contain the so-called extreme-pressure (EP) or anti-wear (AW) additives to reduce the issues characterizing boundary lubrication help protect surfaces if full films cannot be achieved. These additives protect the surfaces from wearing adhering to them and forming a sacrificial sheet.

Mixed lubrication when $h \sim R_a$.

If bearing surface micro asperities contact intermittently, the lubrication regime is the mixed one. This lubrication regime is intermediate between the full film and the boundary lubrication. Also in mixed lubrication additives play an fundamental role in protecting the surfaces.

The three different lubrication regimes can be visibly attributed to different regions of the so-called Stribeck curve illustrated in **Figure 16** adapted from [66]. The curve represents the relationship between the coefficient of friction and the dimensionless Hersey number H defined as:

$$H = \eta \cdot N/F \quad (16)$$

where η is the dynamic viscosity of the lubricant, N the rotation speed and F the normal load.

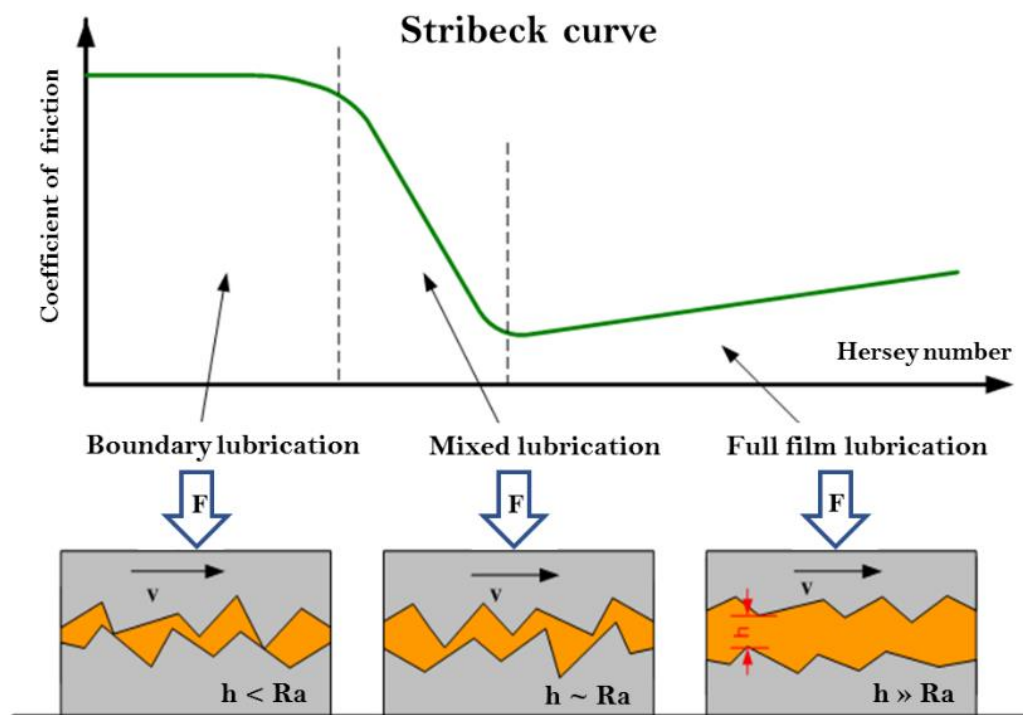


Figure 16 Illustration of the Stribeck curve and the three corresponding lubrication regimes where h is the fluid film thickness and Adapted from [66].

Finally, a wide variety of lubricants are available ranging from liquid, to solid and gaseous. The most extensively used lubricants are liquid ones. The best performers are the synthetic lubricants; however, they have the major disposal and environmental impact issues.

1.11 Hip prosthesis as a tribological system

As already mentioned the number of primary and revision total hip and knee arthroplasty is progressively growing, burdening on the hospital economy [67]. Moreover, increasingly young and active patients have resorted to this operation, placing the problem of prosthetic wear at the center of attention. Great efforts have been employed in the last years to overcome implants wearing thanks to tribology studies. All this has led to great improvements in the efficiency of medical implants that are more performing, to fewer implants failure and to significant costs reductions.

A tribosystem consists of four main elements: a body, an interacting body in relative motion, an interfacial medium and the surrounding environment.

Among the variables characterizing the system there are the relative kinematics of the bodies, the contact load, the load profile and the ambient temperature. The relative movement between two bodies is always accompanied by a loss of energy mostly in the form of heat, sound and wear. The loss of material due to wear, is influenced by several factors such as the diversity of the materials, the surface characteristics (hardness, roughness, surface energy), and by the system conditions such as the presence of lubricant, the type of bodies relative motion and the loads involved. To fully understand wear mechanisms, it is important to know all the mentioned factors. Because of the complexity nature of tribology, hip wear cannot be studied by reference only to the materials properties, but the characteristics of the entire system should be taken into consideration. This system coupling pairs to consider includes the neck-head coupling, the head-acetabular cup pair, and the bone cement-stem coupling. Factors like the contact between the bodies, the fluid at their interface, the temperature, the loads and the movements carried out by the human body influence the conditions of the tribosystem.

Material loss during wear processes is the most important data to be detected in orthopedic applications. Worn material is released in the surrounding tissues in the form of debris that can cause osteolysis and adverse tissue reactions till the prosthesis loosening. A revision surgery is needed to replace the failed implant; this process is still complex, expensive and risky. It has been demonstrated that the

tissue reaction depends on the shape, size and composition of the released particles. For instance, in some cases more particles were released even if the amount of the overall wear was lower. In particular, from the conversion of wear rates and particle size, it has been shown that about $0.2-2 \times 10^{12}$ particles are released per milligram of debris released. Despite the importance of wear, most of the energy dissipated by the system is transformed into heat. Heat generation has been experimentally observed in hip endoprosthesis. In the case of couplings with very small contact areas, as in the case of the modular neck, temperatures can reach up to $60\text{ }^{\circ}\text{C}-80\text{ }^{\circ}\text{C}$. These temperature peaks can encourage chemical reactions and the subsequent deposition of reaction products on the acetabular cup and on the prosthetic neck. This phenomenon explains as well the detected presence of a torque at the level of the prosthetic neck which sometimes, in the presence of large devices, can lead to the unscrewing of the prosthesis. On the other hand, the deposition of reaction products on the implant surfaces has a positive effect for wear resistance. This is because the original surface of the material is transformed into a hybrid one, characterized by the presence of nano-structured crystals, oxidized wear debris and organic material coming from the body fluids that contribute to protect the underlying material [68].

At present, to validate a prosthesis, one of the fundamental pre-clinical evaluations is the wear rate. Laboratory wear tests employ materials and designs utilized in hip prosthesis to get a quality control and to acquire additional information about the tribological mechanisms in joint implants. The main target of laboratory wear tests is to obtain data on wear rate and its dependency on the surrounding environment, such as temperature, loads, lubricant, type of motion. To acquire values that are representative of reality, it is possible to conduct the wear test by reproducing the *in vivo* conditions. The consistency of the obtained results depends on the fidelity in reproducing *in vitro* the human body conditions at the prosthetic level.

1.11.1 Hertz contact theory

When considering a tribosystem, it is fundamental to know the load and the stresses acting at the contact surfaces. Hertz theory (1882) is a theory of contact mechanics that allows to calculate these pressures and it was obtained from the analytical

solution of the equations of elasticity theory [69], [70]. The theory is based on simple analytical equations linking the systems properties to the stresses generated. Tensions and deformations that are produced by pressing two curved elastic bodies against each other can be determined. When two curved bodies are pressed together, the contact zone, initially a point (for spheres) or a line (for cylinders), becomes a finite area due to elastic deformation. Since these surfaces contacts are generally small, the mutual pressures are high and a triaxial state of stress is generated.

The hypotheses at the basis of this theory are:

- Perfect elasticity of materials;
- Absence of friction forces (only normal stresses will be transmitted between the two contact bodies);
- Small contact surface compared to the size of contact bodies.

Since the chosen test configuration in this work is of the cylinder-on-plane, below are reported the equations relative to this case.

1.11.2 Cylinder-on-plane contact

For these two types of contact bodies, the same equations developed for the cylinder-cylinder contact are utilized, considering infinite the diameter of the second cylinder (see **Figure 17**). Consider two elastic solid cylinders into contact on which acts the force F uniformly distributed along the cylinder length l . The contact stress has an elliptical profile across the contact zone wide $2b$.

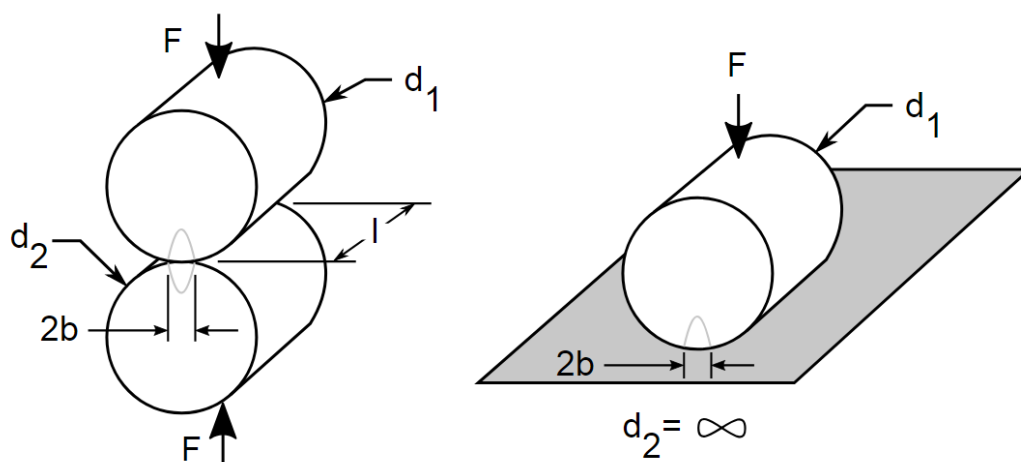


Figure 17 Cylinder-on-plane contact scheme [Estiven R. Sierra, 2015].

The pressure exerted by the force F causes the line of contact to become a rectangle of halfwidth b given by the equation:

$$b = K_b \sqrt{F} \quad (17)$$

where

$$K_b = \left[\frac{2}{\pi l} \frac{(1 - \nu_1^2)/E_1 + (1 - \nu_2^2)/E_2}{(1/d_1) + (1/d_2)} \right]^{1/2} \quad (18)$$

In our case the diameter d_2 of the second cylinder is infinite as showed in the Figure. The terms ν_1 and ν_2 are the Poisson's ratios of the cylinder 1 and cylinder 2 that in this study are respectively the titanium cylinder and the UHMWPE disc, while E_1 and E_2 are their Young's moduli. The other terms appearing in the equation are defined in the Figure.

The maximum contact pressure P_{max} acting between the cylinders along a longitudinal line at the center of the rectangular contact area, is expressed by:

$$P_{max} = \frac{2F}{\pi b l} \quad (19)$$

These equations will be utilized in the experimental section to calculate the pressure between the titanium cylinders and the polyethylene discs in order to match the state of stress encountered in human femoral hips.

In fact, as it will be described in the experimental section, in this work all the precautions to accurately represent the *in vivo* conditions were adopted.

2 EXPERIMENTAL SECTION

At present, the amount of infection occurring in THA and TKA during the first two years is about 1 and 2% respectively, which means around 4000 to 8000 infected implants require surgical revision annually [71]. Infection number, after surgery revision is considerably higher (from 5 to 40%). This burden on patients in terms of well-being as well as on healthcare economy [72].

Infections can be stopped by means of adequate antibiotics supply in the surrounding region of the implantation during the first couple of weeks after surgery. This can be fulfilled through releasing proper drugs *in situ*, which can be stored in micro-dimples textured on the femoral head.

In this work UVT is utilized to create dimples on the surface of Ti6Al4V cylinders that are then tested in a cylinder-on-disc configuration, with UHMWPE as counterpart material, to evaluate both their tribological behaviour and their potentiality as drugs reservoir as a function of time. A lubricated environment was also designed to reproduce more accurately the human body conditions. Results are then compared to the ones obtained with a smooth surface, which is the current finishing condition for the commercially available metal heads.

2.1 Materials

One of the most promising hard-on-soft bearing surfaces employed in hip replacements is the couple Ti6Al4V titanium alloy for the metal head and the ultra-high molecular weight polyethylene (UHMWPE) for the acetabular cups.

In this study, the ISO5834/2 resin GURTM 1050 UHMWPE was used, supplied by OrthoplasticTM in form of bars of 60 mm diameter and 1000 mm length. The UHMWPE bars were machined in order to get a surface finish comparable to that of a commercially available acetabular cup shown in **Figure 18a** (average surface roughness S_a equal to $0.97 \pm 0.04 \mu\text{m}$). After a roughing step to achieve a diameter of 40 mm, a face turning finishing operation was carried out, using feed equal to 0.05 mm and cutting speed equal to 80 m/min. Finally, discs 5 mm thick were cut from the machined bars. **Figure 18b** shows that the machined UHMWPE discs have

a surface finish comparable to that of the acetabular cup, proving their applicability as counterpart material of Ti6Al4V cylinders during the wear experiments.

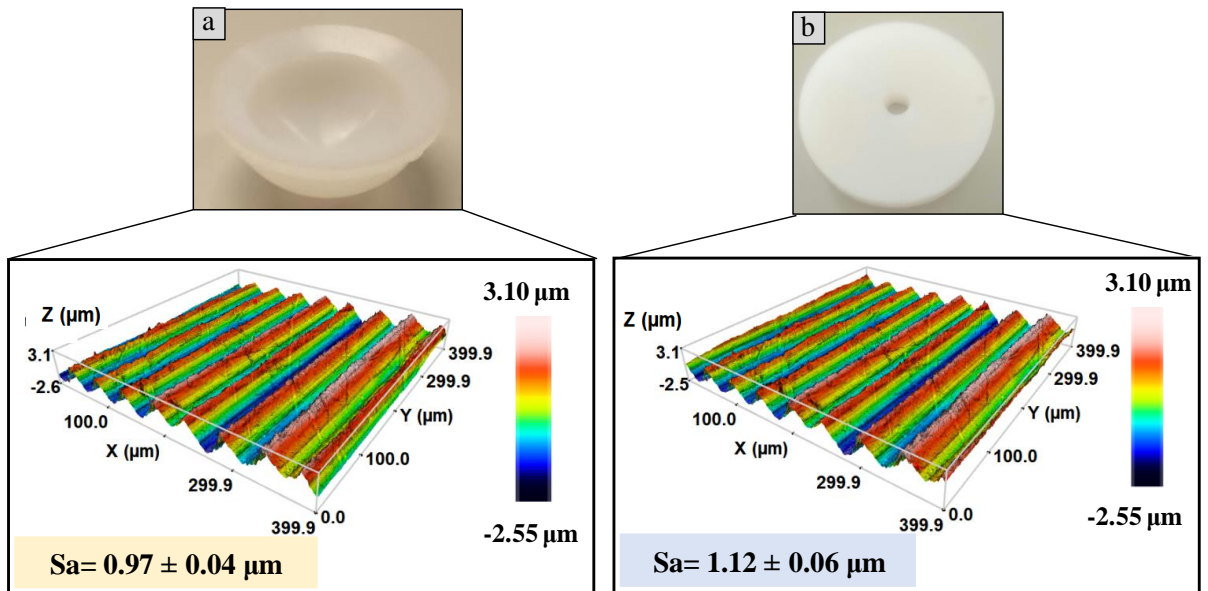


Figure 18 Surface topography of a commercially available acetabular cup (a) and of a machined UHMWPE disc (b).

The Ti6Al4V titanium alloy was provided in form of bars of 40 mm diameter and 180 mm length, from which 4 mm thick cylinders were machined to be used in wear test.

Table 3 reports the main mechanical characteristics of the materials used in the present study.

Table 3 Mechanical characteristics of the tested materials in the as-delivered conditions.

<i>Ti6Al4V</i>	<i>E</i> [GPa]	<i>UTS</i> [MPa]	<i>Y</i> [MPa]	<i>Elongation</i> [%]	<i>Poisson's ratio</i>
	115	1020	950	14	0.35
<i>GUR™ 1050</i> <i>UHMWPE</i>	<i>E</i> [GPa]	<i>Density</i> [g/cm ³]	<i>Y</i> [MPa]	<i>Izod notched</i> [kJ/m ²]	<i>Poisson's ratio</i>
	1.2	0.93	0.48	>73	0.46

2.2 Machining

UVT was carried out on a Mori SeikiTM NL 1500 CNC lathe equipped with an ultrasonic vibration cutting apparatus. The experimental UVT setup (see **Figure 19a**) basically consists of a piezoelectric transducer, a sonotrode, a tool tip, a mechanical setup to fit in the turret of the lathe and driving electronics. As can be seen from the scheme of **Figure 19b**, the tool vibrates perpendicular to the feed direction. More details about the experimental apparatus can be found in [51] and in the paragraph 1.9 concerning UVT systems. The vibration frequency, equal to 30 kHz, was kept fixed for all the tests.

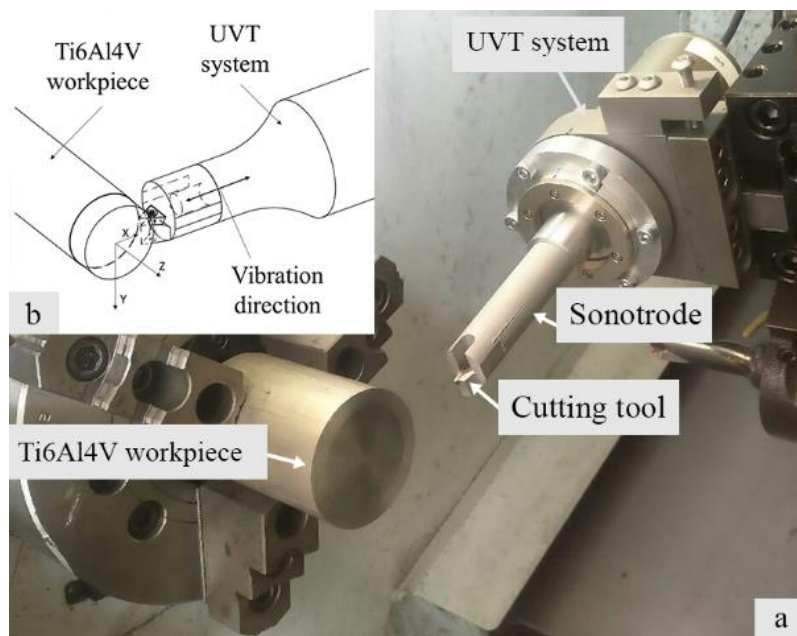


Figure 19 a) Experimental set-up for UVT of the Ti6Al4V cylinders; b) scheme of the UVT setup.

A DCGT 11 T3 08-UM GC1105 coated tungsten carbide insert was used for machining, supplied by Sandvik CoromantTM. A fresh cutting edge was adopted for each test, in order to avoid the influence of the tool wear on the machined surface characteristics.

Before UVT, the Ti6Al4V bars were prepared with a conventional turning finishing pass to achieve a diameter of 19.3 mm, using the same UVT system where ultrasonic vibration was turned off. Later, the ultrasonic vibration assisted a finishing pass, where a depth of cut equal to 0.05 mm was set to reach a final

diameter of 19.2 mm. In order to evaluate the effect of dimples shape on the Ti6Al4V wear behaviour, different cutting speeds were adopted, namely 100 m/min and 200 m/min, whereas the feed was kept fixed and equal to 0.05 mm/rev. The tests were performed under dry conditions and repeated six times for each cutting parameter.

Since the aim of this work is to assess if UVT can represent a valid alternative to machine metal femoral heads, usually polished before being put in service, some Ti6Al4V cylinders were polished to achieve a mirror like surface finish after conventional turning. To do so, the cylinders were ground using up to 4000 SiC grit paper, and then polished using a 1 μm diamond paper and a SiO_2 colloidal dispersion (0.2 μm) in demineralized water and H_2O_2 .

Table 4 summarizes the experimental plan adopted for the machining processes.

Table 4 Experimental plan adopted for turning machining processes.

<i>Test ID</i>	<i>Finishing operation</i>	<i>Cutting speed [m/min]</i>	<i>Depth of cut</i>	<i>Feed</i>	<i>Cooling condition</i>
Smooth	polishing		\		Dry
UVT-100	UVT	100	0.05	0.05	Dry
UVT-200	UVT	200	0.05	0.05	Dry

2.3 Microstructural and mechanical characterization after machining

Samples were cut from the Ti6Al4V machined cylinders for metallographic investigations. After hot mounting into an epoxy resin, grinding and polishing, the Kroll's etchant was used to reveal the grain boundaries. The microstructure was observed using a Leica™ DMRE optical microscope equipped with a high definition digital camera.

Vickers micro-hardness measurements were performed using a Leitz™ Durimet micro-hardness tester with a load of 10 (± 0.5) gr for 30 s; three values were recorded for each measurement point and the average value reported. The hardness

measurements were taken every 20 μm from the machined surface to a depth of 200 μm .

2.4 Contact angle measurements

The measure of the contact angle to evaluate the wettability of the Ti6Al4V machined cylinders was carried out applying a static sessile drop technique. The experimental apparatus consists of a horizontal stage to place the sample, which allows to be adjusted in the vertical direction, a micrometer syringe to form a liquid drop, a halogen and intensity adjustable light source to illuminate the sample, and a Prosilica GTTM camera for the images acquisition. Before measuring, the samples were cleaned in an ultrasonic bath for 15 minutes to remove any residue. A liquid droplet of distilled water characterized by a volume of 10 μL was let fall on the lateral surface of the cylindrical sample. The measurements were conducted at room temperature (25°C); each experiment was repeated eight times to assure reproducibility and the mean value of the experimental results calculated.

2.5 Surface topography analysis after machining

The surface topography of the Ti6Al4V machined cylinders was inspected using a SensofarTM PLu-Neox optical profiler with a 20x magnification NikonTM confocal objective. Data processing, filtering and evaluation of the surface texture parameters were performed according to the ISO 25178 series [73]. On the basis of a previous experimental work [74], the following surface texture parameters were considered:

- Arithmetical mean height of the scale-limited surface (S_a), the most popular areal parameter, which represents the baseline for comparison with other research works.
- Reduced dale height (S_{vk}), an effective parameter to describe the relevance of valleys that can affect the fluid retention in wet applications.
- Reduced peak height (S_{pk}), a parameter giving information about the damaging top portions of the surface that influence the initial sliding during wear tests when the peaks are gradually worn out.

- Skewness of the scale-limited surface (Ssk), showing whether a surface is dominated by peaks or valleys, thus measuring the symmetry of the profile about the mean line.

Besides the above-mentioned surface texture parameters, two additional indicators were taken into account, namely the Aspect Ratio (AR) of the dimples and the density of the dimples (Sdd), with the aim of characterizing the UVT-induced texture.

AR refers to the ratio between the dimples depth and the mean diameter. The dimples average depth was calculated on the basis of three measurements of depth taken on the 2D profile, which was extracted from the 3D topography of the machined surface at six fixed coordinates. For this calculation three different topographies were considered for each cutting condition. The dimples diameter d_{gap} is considered equal to the distance d_{cutt} between two subsequent dimples already defined in equation 4.

The density of the dimples (Sdd) refers to the number of dimples per unit area and it is equivalent to the density of the peaks parameter (Spd) evaluated on a topography symmetric with respect to the Y-axis, that one of the cutting direction.

2.6 Wear tests

To investigate the tribological performances of the couple Ti6Al4V-UHMWPE, the Universal RtecTM tribometer was used (see **Figure 20**). A cylinder-on-disc configuration, in which a Ti6Al4V cylinder was made to slide on a UHMWPE disc, was adopted for the wear tests. A circular multidirectional motion was preferred to linear reciprocating motion in order to mimic the quasi-elliptical path encountered during the *in-vivo* gait [75] and to prevent the alignment of the polymer chains and its consequent strain hardening [76]. Tests were performed in saline solution at 37 ± 1 °C, constantly monitored through a thermometer immersed in a basin filled with water. The experimental setup is shown in **Figure 20**.

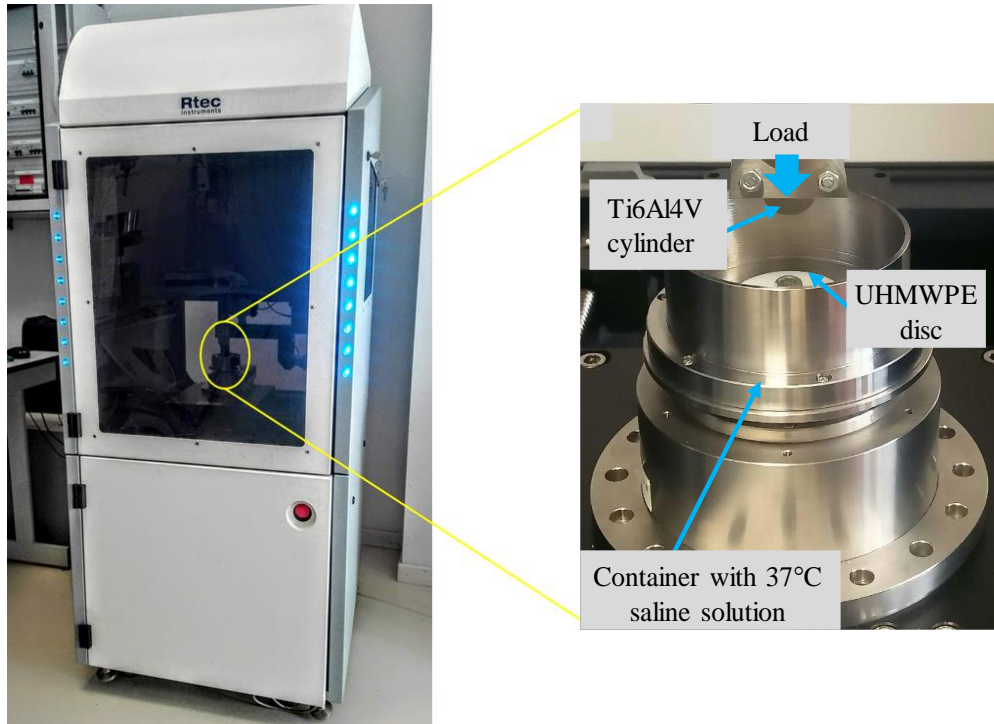


Figure 20 Rtec™ tribometer utilized for wear test and a zoom of the experimental setup.

2.6.1 Setup design

In order to perform the tests with a correct configuration, the setup was specially designed for the supplied Rtec™ tribometer.

The experimental apparatus consists of a basin and a clamp system for the titanium cylinder modeled using the commercial software PTC Creo 3.0®. Simplicity and efficiency have been pursued to achieve a functional test apparatus in a short time. To clamp a titanium cylinder, it was designed a system composed of two symmetric metal blocks with a hollow each as a support seat for the cylinder. The two blocks were then tightened by means of two bolts. The cylinder holder was connected to the load cell of the instrument by means of a pre-existing pin with a threaded hole, through a central screw in a supporting metal disc. The 3D rendering is showed in **Figure 21**.

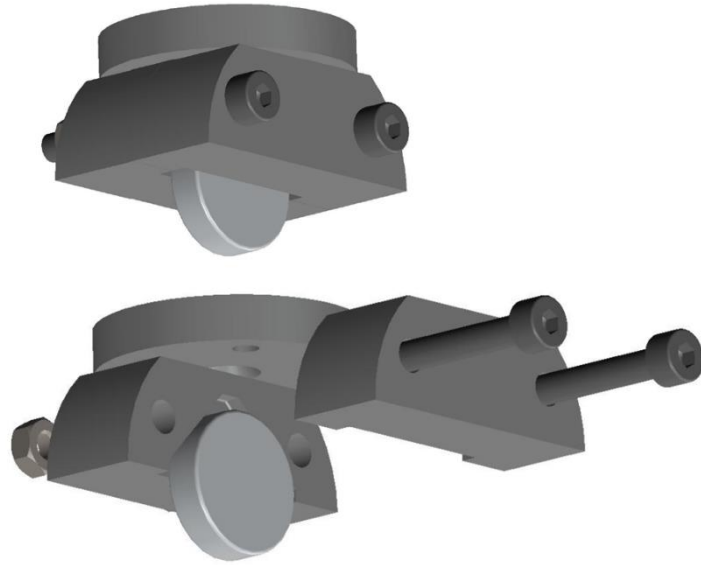


Figure 21 3D rendering of the clamp system for the titanium cylinder, assembled and exploded views are reported.

The basin was designed in order to fit the pre-existing holes on the tribometer base plate and to allow the mechanical fixing of the UHMWPE disc at its base. For this purpose, a central threaded hole and a smooth hole for the plug were machined on the bottom of the basin. Moreover, a drain hole was designed to allow the saline solution change. The 3D rendering of the lower setup is showed in **Figure 22**.

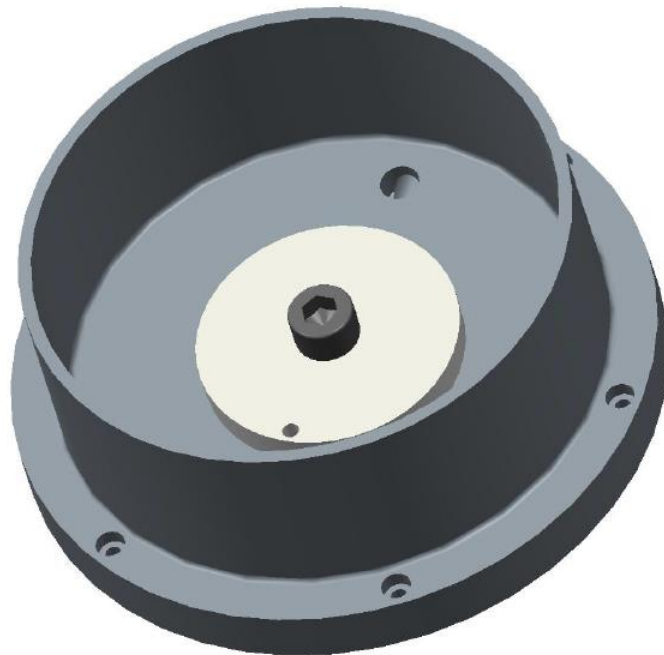


Figure 22 3D rendering of the basin assembled with the UHMWPE disc.

All the above-mentioned components were made of AISI 316L to resist saline solution corrosion that was utilized as lubricant medium.

2.6.2 Wear test parameters

The load was varied during the test to better simulate the load distribution during the human gait. In particular, the circular motion, with a radius of 14 mm at angular speed of 50.3 rad/s, was divided into two parts in which the load was set to 20 ± 1 N and 40 ± 1 N corresponding to 15.8 MPa and 22.3 MPa respectively according to the Hertz theory equations (17), (18) and (19) reported in paragraph 1.11 and using the material properties reported in **Table 3**. The chosen force values were in agreement with the calculations made by Borruto [77]. Below is reported the reasoning that was made.

A typical radius r of metal femoral heads is 14 mm thus, the spherical surface is $4\pi r^2 = 2463 \text{ mm}^2$. The real bearing surface is just a percentage of the total spherical head surface, estimated to be approximately 30%, thus $2463 * 0.3 = 739 \text{ mm}^2$. Taking into consideration a person with a body weight of 70 kg, it is found that median peak forces increase up to seven times the body weight during some activities such as running or going up and down the stairs. Therefore, the maximum load to take into account is 500 kg. The weight per square millimeter will be: $500/739 = 0.68 \text{ kg/mm}^2$. Supposing in first approximation a contact area in our cylinder-on-disc coupling equal to one square millimeter the load results 0.68 kg. Assuming a safety factor of 3 and 6 to take into account possible strikes to the joint, the loads to set in the tribometer have to be $0.68 * 3 = 2 \text{ kg} \approx 20 \text{ N}$ and $0.68 * 6 = 40.8 \text{ kg} \approx 40 \text{ N}$.

With the aim to evaluate the resistance of the textured Ti6Al4V to wear, two different typologies of wear tests were carried out, here called “one-month test” and “three-months test”. The first lasted 94 minutes, equivalent to a period of one month after implantation, while the second type of test lasted 282 minutes, equal to three-months after implantation. These calculations were made according to the assumption that a normal weight person (70 kg), after a hip joint replacement, is medically recommended to perform moderately intense walking that consists of approximately 30 min per day and 50 gait cycles per minute [78]. To reduce the test

duration, the load frequency was speed up to 8 Hz; anyhow, this fixed value of load frequency does not interfere with the experiment according to the ISO 7206/3 standard [79].

The one-month test was performed to evaluate the resistance of the UVT-induced texture to the wear process, since this texture have to be able to endure at least one month to keep drugs that can fight early post-operative infections, which may develop during the first month after implantation [80].

On the other hand, the three-months tests were performed to investigate the actual wear performances of the textured samples, since wear after one-month test was almost negligible and impossible to measure precisely.

Furthermore, to consider the oscillatory characteristic of the joint movements, a variation of the rotational direction was adopted, as half cycle under a given load was made counter clockwise.

A scheme of the executed wear tests is reported in **Figure 21**. Tests were repeated three times for each condition.

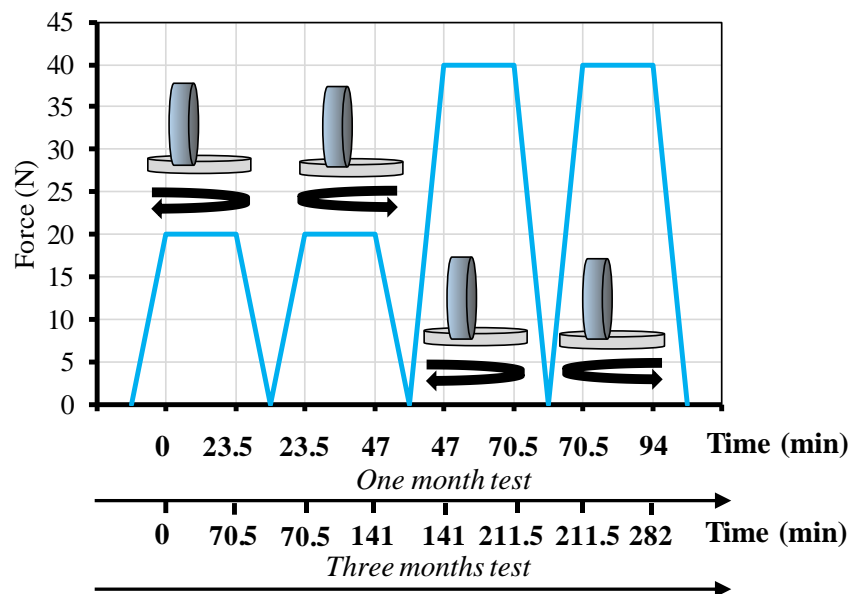


Figure 23 A scheme of the two types of executed wear tests.

2.7 Characterization after wear tests

The surface topography of the worn surfaces of both the Ti6Al4V cylinders and UHMWPE discs were evaluated using the 3D optical profilometer. For the latter, the topographies were taken in correspondence of four reference points. Then, in order to assess wear volume, 2D profiles of the wear track were extrapolated and the area of the wear track was calculated. The average cross section of the worn area was then multiplied by the circumference length in order to assess the wear volume of the UHMWPE.

The FEI™ QUANTA 450 SEM, equipped with the Everhart-Thornley Detector (ETD) and the Back Scattered Electron (BSE) one, was used to examine the surface characteristics of both the worn Ti6Al4V cylinders and UHMWPE discs. Before inspection at Scanning Electron Microscope (SEM), the UHMWPE discs were coated with gold to make them conductive. The gold coating was deposited using a Denton Vacuum™ Desk V machine, with a current of 15 mA for 120 s.

3 RESULTS AND DISCUSSION

3.1 Microstructural and mechanical characteristics of the machined samples

Figure 24 shows the microstructure of the cross section of Ti6Al4V cylinders below the machined surfaces under the investigated cutting conditions.

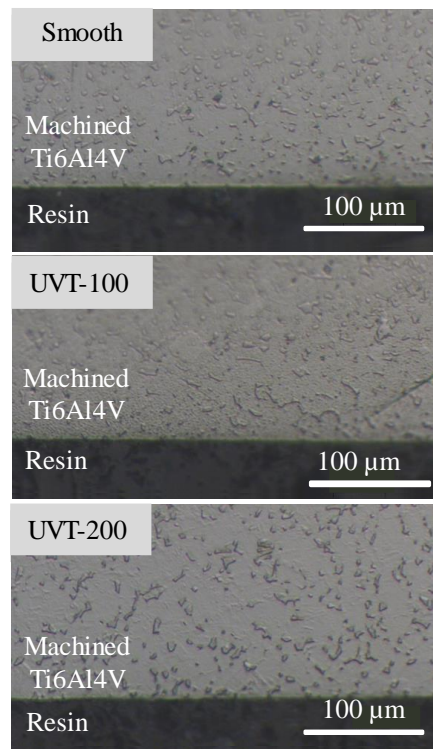


Figure 24 Ti6Al4V cylinders microstructures below the machined surface for the investigated samples.

The presence of a machining-altered layer, namely grains elongated along the cutting speed direction, could not be evidenced, nor phase transformations were detected. As a matter of fact, the temperature arisen during cutting operations was not sufficient to induce any kind of phase transformation in the Ti6Al4V alloy [81]. Micro-hardness measurements confirmed the microstructural evidences (see **Figure 25**), since no evident hardening was found in any of the machined samples. All the measured hardness values are in fact comparable to that of the bulk region. The absence of strain hardening was expected in the polished sample as the heat increase in the cutting zone counteract the effect of strain hardening induced by cutting. On the contrary, the vibration induced by cutting tool on the UVT samples should have amplified the material strain with a consequent expected increased

hardening [82]. However, the absence of strain hardening in the UVT-ed samples can be ascribed to the temperature increase due to the tool ultrasonic motion that exceeded the strain hardening effect of machining operation.

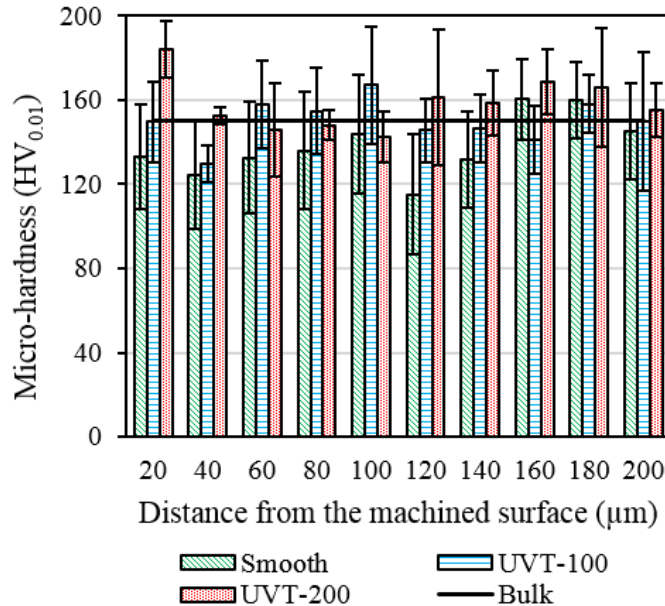


Figure 25 Ti6Al4V cylinders micro-hardness as a function of the distance from the machined surface.

3.2 Wettability results

Figure 26 shows water droplets made to fall on the cylindrical surfaces as a function of the machining parameters. Surface wettability is an important factor since it plays a fundamental role in the biological response of the implant/bone and implant/soft tissue interfaces [83]. As the obtained contact angles are strictly related to the surface topography, it was inspected if the machining-induced topography could affect in a negative way the hydrophilic nature of titanium. The obtained results show that the contact angle was not affected by the fully different surface topographies, therefore it can be stated that UVT did not alter the Ti6Al4V wettability characteristics.

As can be seen from **Figure 26**, only slightly differences can be appreciated between UVT-ed samples. In fact, the cutting speed mainly determines the dimple gaps in the cutting direction, therefore it has a limited impact on the contact angle in the feed direction. These findings are confirmed by a previous research study [84].

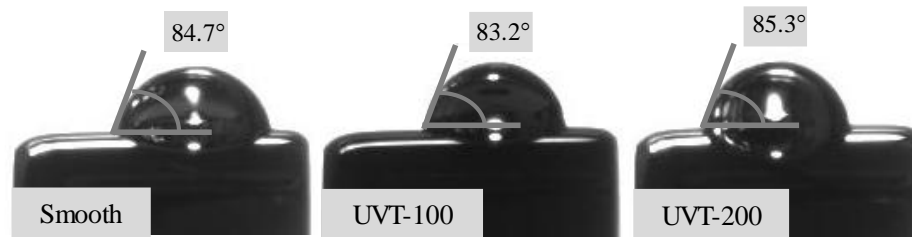


Figure 26 Water droplets on the surfaces of the Ti6Al4V machined samples.

3.3 Surface topography before and after wear

Figure 27 depicts partial profiles of the titanium surfaces measured after machining to evidence the differences in material distribution between the smooth, UVT-100 and UVT-200 samples. Cutting speed is responsible for the distance between the cavities along the cutting direction, as predicted by equation (4). The distance between two subsequent dimples is $55\ \mu\text{m}$ for the UVT-100 sample and $111\ \mu\text{m}$ for the UVT-200 one. **Figure 27** shows also how the texture realized on the surface is regular and the pattern is repeated periodically, proving that the designed requirements of the UVT system are respected.

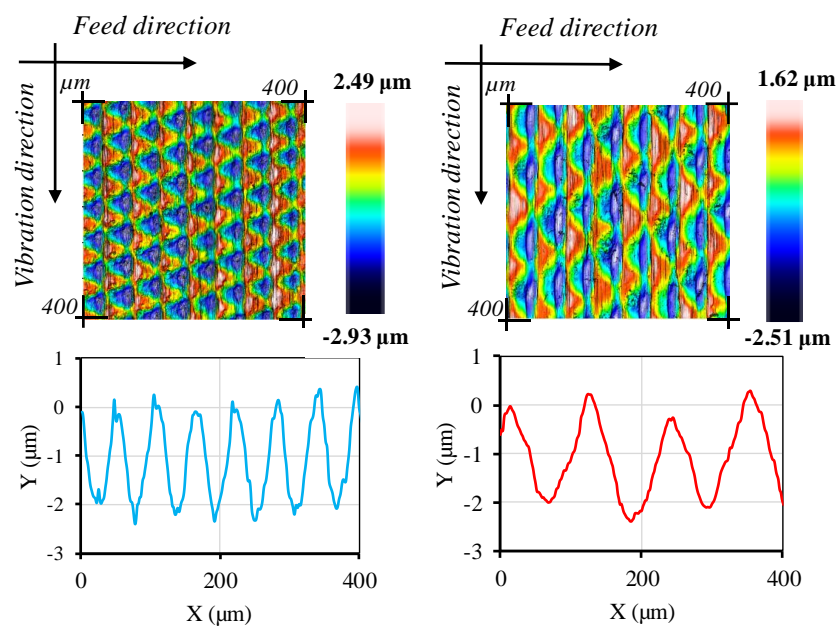


Figure 27 3D topographies and relative 2D profiles of the UVT-100 (left), and UVT-200 (right) samples.

Figure 28 reports the values of the surface texture parameters before and after wear testing. As expected, polishing induced a decrease of all the considered texture parameters, with the only exception of skewness, which set to a value comparable to that of UVT-ed samples. It is worth to note that low skewness values are beneficial for wear applications [85]. Focusing on the difference between the UVT-100 and UVT-200 samples before wear testing (see Fig. 26a), it can be seen that the former was characterized by both higher peaks (*Spk*) and deeper valleys (*Svk*) together with higher surface roughness *Sa*. The aspect ratio of the UVT-100 sample peaks is three times higher than the one obtained with a doubled cutting speed; this means that the peaks are leaner, confirming the surface texture measurements (see **Table 5**). The UVT-100 sample shows also a higher dimples density: this well reflects the fact that in the same area, at a constant feed, the number of valleys in the UVT-200 sample is exactly the half.

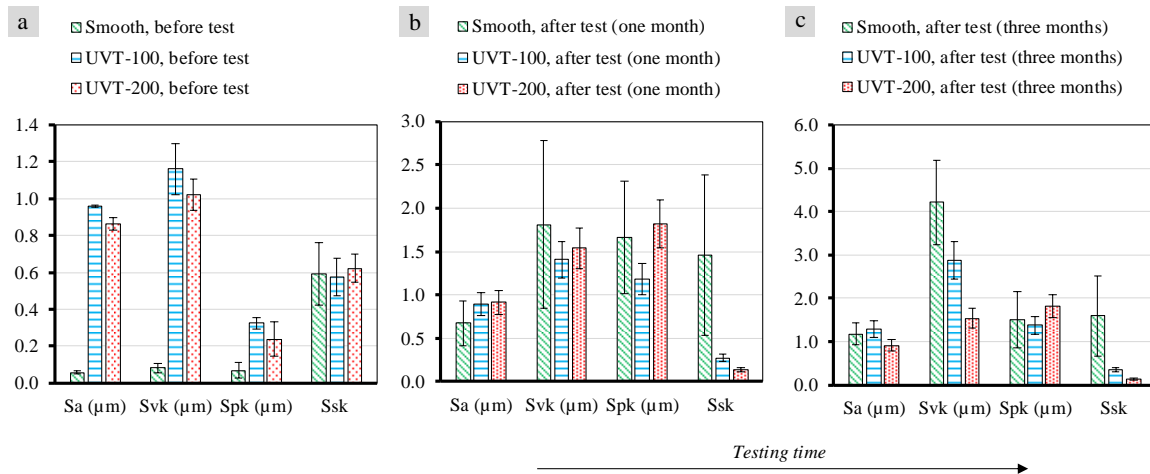


Figure 28 Surface texture parameters of the Ti6Al4V samples before and after wear testing.

After wear testing, the smooth surface was subjected to a drastic increase of *Sa* (see **Figure 28b** and **c**), as a consequence of the presence of wear particles that were trapped between the mating surfaces resulting in a third-body wear mechanism and thus provoking a surface roughness increase. On the contrary, both the UVT-100 and UVT-200 samples showed a reduction of *Sa* as a consequence of the flattening of the sliding interfaces [50].

For all the samples, regardless of the initial state, a drastic increase in the values of *Spk* and *Svk* was noticed after wear testing. Looking at the 2D profiles extracted

from the surface topography of the UVT-100 and UVT-200 samples (**Figure 29**), it can be seen that the profiles were affected by the wear process, being patchier and more irregular. Again, the skewness of the smooth sample showed a particular behaviour, settling to higher values compared to the one of the other samples. From those considerations, it can be concluded that, just after a month, the smooth surface changed completely its characteristics, achieving roughness values comparable to those of the UVT-100 and UVT-200 samples. On the contrary, the unique surface roughness induced by UVT was preserved.

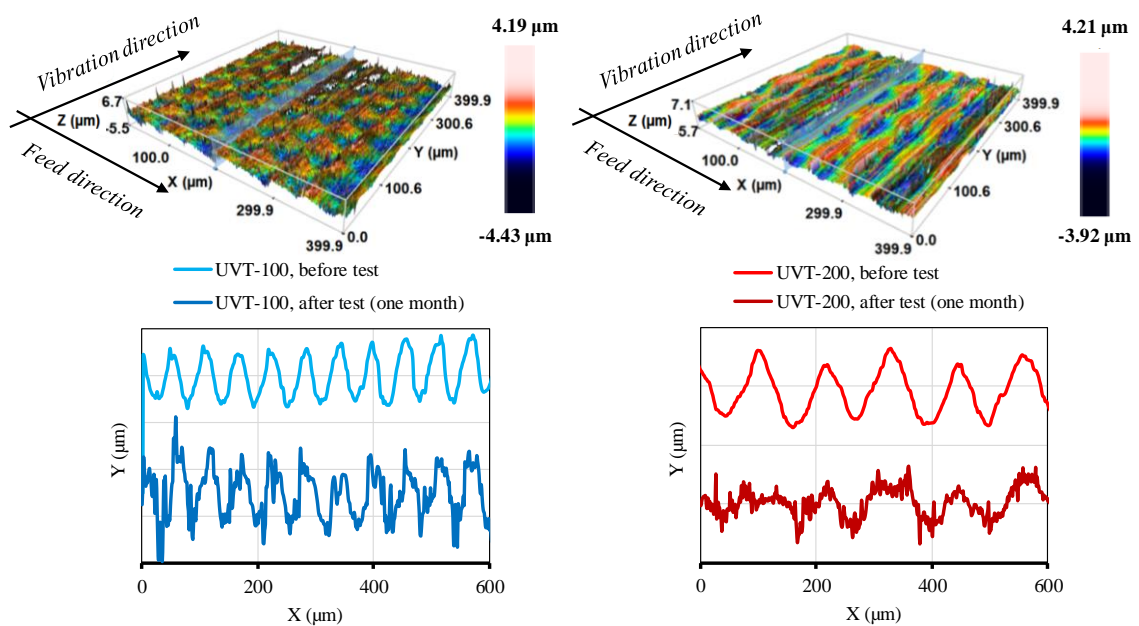


Figure 29 3D topographies and relative 2D profiles after one-month testing of the UVT-100 (left), and UVT-200 (right) samples.

After three-months wear testing, S_a and S_{sk} were slightly influenced by the wear process compared to the ones of the one-month tests for all the investigated samples, indicating that almost stationary values were achieved. On the contrary, S_{pk} and S_{vk} were influenced by the wear process, being much more sensible to the wear phenomena, namely abrasion and adhesion. In particular, a drastic increase of S_{pk} was found for the UVT-200 sample, while a drastic increase of S_{vk} was detected for both the smooth and UVT-100 samples.

Table 5 shows that the UVT-100 sample, characterized by higher AR values just after machining, preserved in a more efficient way its initial valleys configuration

compared to the UVT-200 sample. As a consequence, it can preserve valleys for a longer time compared to the other sample. Actually, the AR increase after one-month wear testing is equal to 14% for the UVT-100 sample and 200% for the UVT-200 one. It is worth to note that the AR measurements after wear testing are affected by some uncertainty due to the samples jagged profiles and therefore the reported values are only indicative. This is the reason why AR and dimples density values were not calculated for the three-months wear tests.

The density of dimples *Sdd* showed a dramatic increase for both samples after wear testing, which means that this parameter cannot be considered reliable for describing the characteristics of worn dimples. This can be explained with the fact that, by mirroring the surface to the axis of the cutting direction, the presence of localized scratched areas played a major effect in the *Sdd* calculation. For this reason, the *Sdd* values after one month wear testing are not reported in **Table 5**.

Table 5 Aspect ratio and density of the dimples of the UVT samples before and after wear testing.

	<i>Before wear testing</i>		<i>After one-month wear testing</i>	
	AR	Sdd	AR	Sdd
UVT-100	0.036 ± 0.5	385 ± 2	0.041 ± 0.1	/
UVT-200	0.01 ± 0.4	189 ± 9	0.03 ± 0.1	/

On the basis of the aforementioned results, UVT-100 condition appears to generate the surface texture most appropriate for the purpose of this thesis.

3.4 Tribological results

Table 6 shows the average Coefficient of Friction (COF) values acquired during wear testing at varying load as a function of test duration. In case of the tests lasting one month with the application of a load of 20 N, the UVT-100 and UVT-200 samples showed a reduction of 25% of the friction coefficient compared to the one of the smooth surface. Three-months wear tests showed a further reduction, which was more significant in case of the UVT-100 sample. When the load was increased to 40 N in the one-month test, the UVT-100 and UVT-200 samples showed a reduction of 41% and 17% compared to the smooth one, respectively. Quite the

same reduction in COF was found in the case of tests lasting three-months and with the same applied load. In general, it can be stated that the smooth surface always presented the highest friction coefficient regardless of the load.

Table 6 Average friction coefficients as a function of load and test duration.

	<i>One-month wear testing</i>		<i>Three-months wear testing</i>	
	20 N	40 N	20 N	40 N
Smooth	0.16 ± 0.05	0.17 ± 0.01	0.21 ± 0.02	0.19 ± 0.001
UVT-100	0.12 ± 0.04	0.1 ± 0.02	0.13 ± 0.01	0.13 ± 0.001
UVT-200	0.12 ± 0.02	0.14 ± 0.05	0.1 ± 0.08	0.16 ± 0.002

Lower friction coefficients are beneficial for ameliorating hip joint performances, since they reduce the frictional force responsible of both polyethylene wear and aseptic loosening [86]. It is well known that friction is influenced by both the surface texture and mechanical properties of the surface and sub-surface [87]. As it was shown in paragraph 3.1, both the micro-hardness and microstructure of the UVT samples were comparable to those of the smooth sample, therefore the decrease of friction coefficient found in UVT samples can be attributable only to the presence of a textured surface. Similarly, different degrees of wettability can induce differences in the friction coefficient. It was shown in [88] that hydrophilic surface texture contributed to shift vertically the Stribeck curve, due to the thicker layer of the fluid film compared to hydrophobic surfaces. Again, it was shown in paragraph 3.2 that the contact angles did not substantially differ, meaning that the friction coefficient reduction can be solely attributed to the presence of a textured surface.

The following main effects of textured surfaces are expected to improve the tribological performance, according to [36], [89], [90]: 1) a textured surface has the ability to trap wear particles, avoiding the presence of debris between the two surfaces, which can cause abrasive or adhesive wear and are involved in three body wear mechanisms; 2) dimples can act as an efficient reservoir, storing wear particles inside the surface cavities, thus making the reduction of abrasive wear conceivable. In addition, it was demonstrated in [91] that a temperature reduction took place in the case of textured surfaces in comparison with polished surfaces, thanks to the

efficient lubrication at the contact points. The latter can cause a softening in the polyethylene discs, increasing the amount of abrasive wear.

Table 6 shows that the UVT samples are sensitive to the load applied during wear testing. When the applied load was 20 N, the different UVT samples showed comparable performances, while, when doubling the load, the friction coefficient of the UVT-100 sample was always lower than the one of the UVT-200 sample. This implies a different load-carrying capacity of the tested surfaces, which may be linked to the higher density of dimples of the UVT-100 sample (see **Table 5**). Chyr et al. [49] demonstrated that the presence of a microstructure on the surface could increase the load-carrying capacity of the lubricant film between two bearing surfaces in relative motion thanks to the increase of the lubricant film thickness and consequent reduction in contact (full film lubrication), thereby reducing friction and potentially wear of the articulating surfaces.

In addition to friction, wear occurring at the mating interfaces was evaluated by means of topography analyses. After the one-month wear tests, only negligible levels of wear were recorded and, therefore, the wear volume calculation was not carried out. On the contrary, **Figure 30** reports the wear volume values of the UHMWPE after the three-months wear tests. Results show that the texturing of the Ti6Al4V cylinders surface did not alter the UHMWPE wear volume, since data referring to testing against smooth and UVT-200 samples have comparable values. The wear volume of the UHMWPE tested against the UVT-100 sample, instead, was the lowest in accordance with the reported friction results.

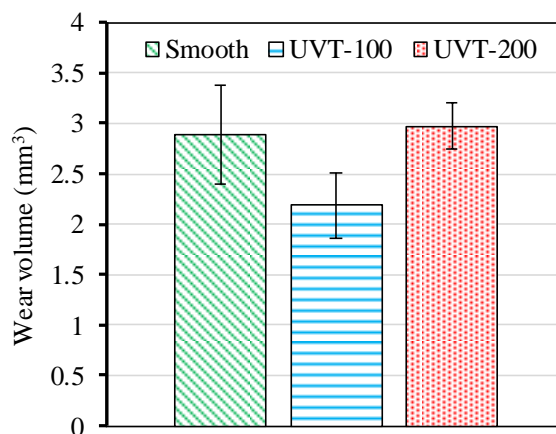


Figure 30 Wear volume of the UHMWPE tested against smooth, UVT-100 and UVT-200 samples after three-months of wear testing.

In a wear process, only the summit points of the surface are in contact to each other, bearing the whole load. Over time and at increasing load, also the lower points of the surfaces come into contact due to the plastic deformation of the asperity areas. Although un-textured surfaces are smoother, the peaks that protrude above the mean line (described by the Ssk parameter) are demonstrated to increase as a consequence of the wear process. On the contrary, the Ssk values of the UVT samples decreased after wear testing, thanks to the presence of the dimples. In particular, the UVT-100 sample presented the highest initial Sdd that is demonstrated to be useful into both friction and wear processes.

3.5 SEM images of wear scars

Figure 31 reports SEM images at different magnification of the wear scars of the Ti6Al4V cylinders after three-months of wear testing. Abrasive wear signs appear as wear scars, clearly visible on the surface of the smooth sample (see **Figure 31a**). As a consequence of the abrasion, flakes of material are removed from the surfaces, together with some wear debris. Actually, a large amount of wear debris particles is found on the smooth sample surface as evidenced in the magnified image of **Figure 31a**. These particles can favour the occurrence of the three-body abrasion phenomenon that may significantly increase the wear rate [50], and are detrimental for total hip replacements since they can elicit a foreign body reaction, resulting in loosening. Moreover, no sign of adhesive wear is noticeable.

On the contrary, wear debris can be trapped inside the valleys present on the UVTeD surfaces. The magnification of **Figure 31b** demonstrates that the surface valleys are completely full of wear particles preventing their harmful role. Traces of adhesive wear are also visible. The presence of adhesion wear can be considered positive as the adhered material can protect underlying layers from further abrasion, reducing the amount and increasing the size of wear particles that can dissipate into the human body. It is worth to note that small wear debris particles are the most dangerous since they can be more easily conveyed by the blood into the body.

The UVT-100 samples seem to have the most efficient micro-structure since the wear particles are collected in a more homogeneous way (see **Figure 31b** compared to **Figure 31c**). This can be attributed to the preservation of the starting microstructure for a longer duration as seen in the 2D profiles of **Figure 29**.

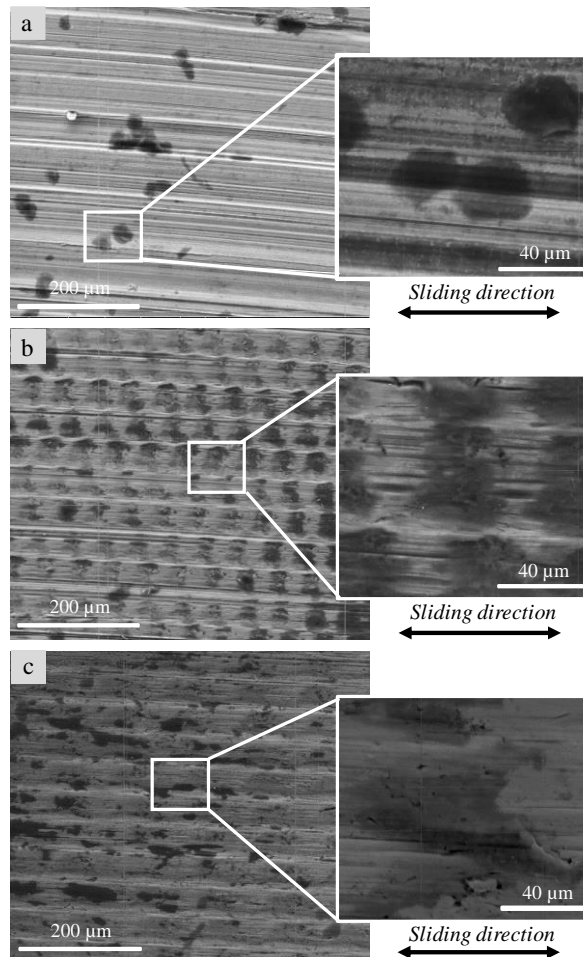


Figure 31 SEM images at different magnification of the worn Ti6Al4V samples after three-months of wear testing: a) polished, b) UVT-100 and c) UVT-200.

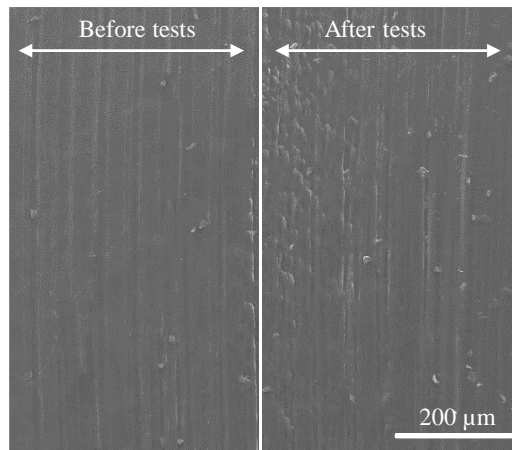


Figure 32 SEM image of worn UHWPE after three-months of wear testing (smooth Ti6Al4V as counterpart material).

Figure 32 shows the comparison between the UHWPE before and after wear tests using the Ti6Al4V cylinder with smooth surface as counterpart material. After testing, parallel ripples with plastically deformed edges together with numerous wear particles were shown. In highly deformed areas, elongated fibrils protrude from the surface [92].

No sensible differences in wear scars on the UHMWPE were found when varying the counterpart material.

4 CONCLUSIONS

The obtained results show that the proposed methodology improves the tribological performances compared to the standard polished surfaces, proving that UVT can be considered a promising manufacturing technique to functionalize the surface of femoral head implants through the creation of micro-dimples for releasing drugs during the first stages of the prosthesis implantation.

In the present study, the effect of surface texturing on the wear performances of the Ti6Al4V-UHMWPE pair was evaluated. Ultrasonic Vibration Turning (UVT) was exploited to create dimples on the surface of Ti6Al4V cylinders, varying the cutting speed in order to modify the distance between subsequent dimples.

Cylinder-on-disc wear tests were used with the objective of evaluating if the surface texture induced by UVT affected tribological performances. Smooth surfaces produced by polishing were chosen as reference.

The main results can be summarized as follows:

- UVT did not affect the Ti6Al4V characteristics in terms of microstructure, micro-hardness and wettability.
- Even if the surface finish of the investigated samples after machining was drastically different, just after a month of wear testing, smooth samples showed a surface roughness comparable to the one of the UVT-ed samples indicating that the smooth texture was lost after few cycles.
- After a month of wear testing, 2D profiles of the worn surfaces of the UVT-ed samples showed that the dimples were partially preserved, therefore, their possible function of drug deliverer was still active. Samples machined by UVT at the lowest cutting speed performed better, thanks to their higher initial aspect ratio and higher density of dimples.
- UVT-ed samples showed a sensible reduction in the coefficient of friction compared to the smooth one, especially the sample machined at the lowest cutting speed.
- Wear volume of the UHMWPE was not affected by the introduction of the UVT-induced texture.

- SEM images of the wear scars after three-months of wear testing confirmed that the UVT dimples were full of counterpart material. This can prove their efficiency in trapping wear debris.
- UVT-ed samples were characterized by both abrasive and adhesive wear; the presence of the latter is positive since it prevents the release of small wear debris particles. On the contrary, smooth surfaces were mostly characterized by abrasive wear and the presence of higher amount of harmful wear particles.

On these bases, it can be concluded that UVT can be a potential manufacturing technology to machine Ti6Al4V metal heads for hip prosthesis creating surface micro-dimples for releasing drugs during the first stages of the prosthesis implantation.

5 LIST OF ABBREVIATIONS

UVT: ultrasonic-assisted vibration turning; **UHMWPE**: ultra-high molecular weight polyethylene; **THA**: total hip arthroplasty; **TKA**: total knee arthroplasty; **PMMA**: poly(methyl methacrylate); **PDMS**: polydimethylsulphoxide; **PEEK**: polyetheretherketone; **HA**: hydroxyapatite; **MOP**: metal-on-polyethylene; **MOXP**: metal-on-crosslinked polyethylene; **MOM**: metal on metal; **COC**: ceramic on ceramic; **hcp**: hexagonal close packed; **bcc**: body-centered cubic; **EBM**: electron beam melting; **PVD**: physical vapor deposition; **FIB**: focused ion beam; **PCE** : photochemical etching; **SB**: shot blasting ; **LSEM** : large strain extrusion machining; **DOC**: depth of cut; **1D**: one dimension(al); **2D**: two dimension(al); **HSR**: horizontal speed ratio; **DC**: duty cycle; **Sa**: arithmetical mean height of the scale-limited surface; **Svk**: reduced dale height; **Spk**: reduced peak height; **Ssk**: skewness of the scale-limited surface; **AR**: aspect ratio; **Sdd**: density of the dimples; **3D**: three dimension(al); **EDT**: Everhart-Thornley detector; **BSE**: back scattered electron; **SEM**: scanning electron microscope; **COF**: coefficient of friction.

6 BIBLIOGRAPHY

- [1] United Nations, “World Population Prospects The 2017 Revision Key Findings and Advance Tables,” *World Popul. Prospect. 2017*, pp. 1–46, 2017.
- [2] W. Khan, E. Muntimadugu, M. Jaffe, and A. J. Domb, “Implantable Medical Devices,” in *Focal Controlled Drug Delivery*, A. J. Domb and W. Khan, Eds. Boston, MA: Springer US, 2014, pp. 33–59.
- [3] V. K. Khanna, “Biomaterials for Implants,” in *Implantable Medical Electronics*, Springer, 2015, p. 153–166.
- [4] L. K. King, L. March, and A. Anandacoomarasamy, “Obesity & osteoarthritis.,” *Indian J. Med. Res.*, vol. 138, no. August, pp. 185–93, 2013.
- [5] J. Holdaway, P. Levitt, J. Fang, and N. Rajaram, “Mobility and health sector development in China and India,” *Soc. Sci. Med.*, vol. 130, pp. 268–276, 2015.
- [6] G. Erens and M. Crowley, “Total hip arthroplasty,” *UpToDate*, pp. 1–19, 2017.
- [7] R. Otten, P. M. van Roermund, and H. S. J. Picavet, “Trends in the number of knee and hip arthroplasties: considerably more knee and hip prostheses due to osteoarthritis in 2030.,” *Ned. Tijdschr. Geneesk.*, vol. 154, no. 2010, p. A1534, 2010.
- [8] S. Nemes, M. Gordon, C. Rogmark, and O. Rolfson, “Projections of total hip replacement in Sweden from 2013 to 2030,” *Acta Orthop.*, vol. 85, no. 3, pp. 238–243, 2014.
- [9] D. Culliford, J. Maskell, A. Judge, C. Cooper, D. Prieto-Alhambra, and N. K. Arden, “Future projections of total hip and knee arthroplasty in the UK: Results from the UK Clinical Practice Research Datalink,” *Osteoarthr. Cartil.*, vol. 23, no. 4, pp. 594–600, 2015.
- [10] B. D. Ulery, L. S. Nair, and C. T. Laurencin, “Biomedical applications of biodegradable polymers,” *J. Polym. Sci. Part B Polym. Phys.*, vol. 49, no. 12, pp. 832–864, 2011.
- [11] M. Niinomi, M. Nakai, and J. Hieda, “Development of new metallic alloys for biomedical applications,” *Acta Biomater.*, vol. 8, no. 11, pp. 3888–3903, 2012.
- [12] S. M. Best, A. E. Porter, E. S. Thian, and J. Huang, “Bioceramics: Past, present and for the future,” *J. Eur. Ceram. Soc.*, vol. 28, no. 7, pp. 1319–1327, 2008.
- [13] P. Y. Chen, J. McKittrick, and M. A. Meyers, “Biological materials: Functional adaptations and bioinspired designs,” *Prog. Mater. Sci.*, vol. 57, no. 8, pp. 1492–1704, 2012.
- [14] J. Park and R. S. Lakes, *Biomaterials*. 2007.
- [15] D. Williams, *The Williams Dictionary of Biomaterials*. Liverpool University Press, 1999.
- [16] J. HUANG, “15 - Cellular response to hydroxyapatite and Bioglass® in tissue engineering and regenerative medicine,” in *Woodhead Publishing Series in Biomaterials*, L. B. T.-C. R. to B. Di Silvio, Ed. Woodhead Publishing, 2009, pp. 371–390.
- [17] T. Hanawa, “Overview of metals and applications,” *Met. Biomed. Devices*, pp. 3–24, 2010.

-
- [18] G. Giarmatzis, I. Jonkers, M. Wesseling, S. Van Rossom, and S. Verschueren, "Loading of Hip Measured by Hip Contact Forces at Different Speeds of Walking and Running," *J. Bone Miner. Res.*, vol. 30, no. 8, pp. 1431–1440, 2015.
- [19] J. Black and G. Hastings, *Handbook of Biomaterial Properties*. London: Chapman & Hall, 1998.
- [20] J. Wolff, *The Law of Bone Remodelling*. Berlin: Springer-Verlag Berlin Heidelberg, 1986.
- [21] and D. G. R. Callister, William D., "Artificial Total Hip Replacement - Case study 4," *Fundam. Mater. Sci. Eng. an Integr. approach.*, vol. 4, pp. 253–254, 2012.
- [22] M. Navarro, A. Michiardi, O. Castaño, and J. Planell, "Biomaterials in orthopaedics," *J. R. Soc. Interface*, vol. 5, no. 27, pp. 1137–1158, 2008.
- [23] M. Hamadouche and L. Sedel, "Ceramics in Orthopaedics," *J. Bone Jt. Surg.*, vol. 82, no. 8, pp. 1095–1099, 2000.
- [24] J. Chevalier and L. Gremillard, "Ceramics for medical applications: A picture for the next 20 years," *J. Eur. Ceram. Soc.*, vol. 29, no. 7, pp. 1245–1255, 2009.
- [25] C. Auclair-Daigle, M. N. Bureau, J. G. Legoux, and L. Yahia, "Bioactive hydroxyapatite coatings on polymer composites for orthopedic implants," *J. Biomed. Mater. Res. - Part A*, vol. 73, no. 4, pp. 398–408, 2005.
- [26] E. L. Steinberg, E. Rath, A. Shlaifer, O. Chechik, E. Maman, and M. Salai, "Carbon fiber reinforced PEEK Optima-A composite material biomechanical properties and wear/debris characteristics of CF-PEEK composites for orthopedic trauma implants," *J. Mech. Behav. Biomed. Mater.*, vol. 17, pp. 221–228, 2012.
- [27] L. L. Hench, "Bioceramics: From Concept to Clinic," *J. Am. Ceram. Soc.*, vol. 74, no. 7, pp. 1487–1510, 1991.
- [28] W. Waugh, *John Charnley: The Man and the Hip. Annals of the Rheumatic Diseases. 1990;49(9)*. Springer, 1990.
- [29] G. E. J. Poinern, R. K. Brundavanam, and D. Fawcett, "Nanometre Scale Hydroxyapatite Ceramics for Bone Tissue Engineering," *Am. J. Biomed. Eng.*, vol. 3, no. 6, pp. 148–168, 2013.
- [30] J. R. H. Foran, "Total Hip Replacement." [Online]. Available: <https://orthoinfo.aaos.org/en/treatment/total-hip-replacement/>. [Accessed: 22-Aug-2018].
- [31] A. W. Gjønnnes, "Effect of Sulfide Inclusions in Austenitic Stainless Steel on the Initiation of Pitting in Base Metal and Heat Affected Zone after Welding," 2012.
- [32] "Titanium," *Encyclopaedia Britannica*, 2018. [Online]. Available: <https://www.britannica.com/science/titanium>. [Accessed: 20-Aug-2018].
- [33] A. Morri, "Trattamenti termici delle leghe di titanio $\alpha+\beta$, correlazioni fra microstruttura e comportamento meccanico," *Metall. Ital.*, vol. 100, no. 10, pp. 1–10, 2008.
- [34] H. J. Rack and J. I. Qazi, "Titanium alloys for biomedical applications," *Mater. Sci. Eng. C*, vol. 26, no. 8, pp. 1269–1277, 2006.
- [35] O. Harryson and D. Cormier, "Direct Fabrication of Metal Orthopedic Implants Using Electron Beam Melting Technology," *Free. Fabr.*, no. Aug, 13, pp. 439–446, 2003.
- [36] A. A. G. Bruzzone, H. L. Costa, P. M. Lonardo, and D. A. Lucca,

- “Advances in engineered surfaces for functional performance,” *CIRP Ann. - Manuf. Technol.*, vol. 57, no. 2, pp. 750–769, 2008.
- [37] C. J. Evans and J. B. Bryan, “‘Structured’, ‘textured’ or ‘engineered’ surfaces,” *CIRP Ann. - Manuf. Technol.*, vol. 48, no. 2, pp. 541–556, 1999.
- [38] J. Aggarwal, A. Kotlicki, M. Mossman, and L. Whitehead, “Liquid transport based on electrostatic deformation of fluid interfaces,” *J. Appl. Phys.*, vol. 99, no. 10, 2006.
- [39] J. H. Yum, S. J. Yoo, S. S. Kim, D. Y. Kim, and Y. E. Sung, “Anti-Reflection Layer Using Nano Structured Surface Relief Gratings for Solar Cell,” in *ECS 203rd meeting*, 2003.
- [40] D. F. Stamatialis *et al.*, “Medical applications of membranes: Drug delivery, artificial organs and tissue engineering,” *J. Memb. Sci.*, vol. 308, no. 1–2, pp. 1–34, 2008.
- [41] P. Wei and G. S. Swei, “PRODUCTION OF LAYERED ENGINEERED ABRASIVE SURFACES,” 2001.
- [42] H. Ohmori, K. Katahira, J. Komotori, and M. Mizutani, “Functionalization of stainless steel surface through mirror-quality finish grinding,” *CIRP Ann. - Manuf. Technol.*, vol. 57, no. 1, pp. 545–549, 2008.
- [43] K. Anagnostakos, N. V Schmid, J. Kelm, U. Grun, and J. Jung, “Classification of hip joint infections,” *Int. J. Med. Sci.*, vol. 6, no. 5, pp. 227–233, 2009.
- [44] T. Bongartz *et al.*, “Incidence and risk factors of prosthetic joint infection after total hip or knee replacement in patients with rheumatoid arthritis,” *Arthritis Rheum.*, vol. 59, no. 12, pp. 1713–1720, 2008.
- [45] C. E. Stake, P. Y. Talbert, W. J. Hopkinson, R. J. Daley, K. J. Alden, and B. G. Domb, “Hip Arthroplasty or Medical Management: A Challenging Treatment Decision for Younger Patients,” *J. Arthroplasty*, vol. 30, no. 6, pp. 950–954, 2015.
- [46] M. T. Mathew, P. Srinivasa Pai, R. Pourzal, A. Fischer, and M. A. Wimmer, “Significance of tribocorrosion in biomedical applications: Overview and current status,” *Adv. Tribol.*, vol. 2009, 2009.
- [47] H. Ito, K. Kaneda, and T. Yuhta, “Reduction of Polyethylene Wear by Concave Dimples on the Frictional Surface in Artificial Hip Joints,” *J. Arthroplasty*, vol. 15, no. 3, pp. 332–338, 2000.
- [48] H. Sawano, S. Warisawa, and S. Ishihara, “Study on long life of artificial joints by investigating optimal sliding surface geometry for improvement in wear resistance,” *Precis. Eng.*, vol. 33, no. 4, pp. 492–498, 2009.
- [49] A. Chyr, M. Qiu, J. W. Speltz, R. L. Jacobsen, A. P. Sanders, and B. Raeymaekers, “A patterned microtexture to reduce friction and increase longevity of prosthetic hip joints,” *Wear*, vol. 315, no. 1–2, pp. 51–57, 2014.
- [50] S. Bruschi, R. Bertolini, A. Bordin, F. Medea, and A. Ghiotti, “Influence of the machining parameters and cooling strategies on the wear behavior of wrought and additive manufactured Ti6Al4V for biomedical applications,” *Tribol. Int.*, vol. 102, pp. 133–142, 2016.
- [51] E. Di Iorio, R. Bertolini, S. Bruschi, and A. Ghiotti, “Design and development of an ultrasonic vibration assisted turning system for machining bioabsorbable magnesium alloys,” *Procedia CIRP*, 2018.
- [52] S. Amini, H. N. Hosseinabadi, and S. A. Sajjady, “Experimental study on effect of micro textured surfaces generated by ultrasonic vibration assisted

- face turning on friction and wear performance,” *Appl. Surf. Sci.*, vol. 390, pp. 633–648, 2016.
- [53] D. Xing, J. Zhang, X. Shen, Y. Zhao, and T. Wang, “Tribological properties of ultrasonic vibration assisted milling aluminium alloy surfaces,” vol. 6, pp. 539–544, 2013.
- [54] R. C. Skelton, “Turning with an oscillating tool,” *Int. J. Mach. Tool Des. Res.*, vol. 8, no. 4, pp. 239–259, 1968.
- [55] P. M. Rinck, S. Sitzberger, and M. F. Zaeh, “Actuator design for vibration assisted machining of high performance materials with ultrasonically modulated cutting speed,” in *SPIE 10326, Fourth European Seminar on Precision Optics Manufacturing*, 2017.
- [56] D. E. Brehl and T. A. Dow, “Review of vibration-assisted machining,” *Precis. Eng.*, vol. 32, no. 3, pp. 153–172, 2008.
- [57] H. Suzuki, M. B. Marshall, N. D. Sims, and R. S. Dwyer-Joyce, “Design and implementation of a non-resonant vibration-assisted machining device to create bespoke surface textures,” *Proc. Inst. Mech. Eng. Part C J. Mech. Eng. Sci.*, vol. 231, no. 5, pp. 860–875, 2017.
- [58] F. Klocke and O. Rubenach, “Ultrasonic Assisted Diamond Turning of Steel and Glass,” in *American Society of Precision Engineers*, 1998, pp. 179–190.
- [59] E. Brinksmeier and R. Glabe, “Elliptical Cutting of Steel with Diamond Tools,” in *American Society of Precision Engineers*, 1999, pp. 163–166.
- [60] J. Ahn, H. Lim, and S. Son, “Improvement of micro-machining accuracy by 2-dimensional vibration cutting,” *Proc ASPE*, no. 2, pp. 2–5, 1999.
- [61] T. Moriwaki, E. Shamoto, and K. Inoue, “Ultraprecision Ductile Cutting of Glass by Applying Ultrasonic Vibration,” *CIRP Ann. - Manuf. Technol.*, vol. 41, no. 1, pp. 141–144, 1992.
- [62] B. Bhushan, *Principles and Applications of Tribology*. John Wiley & Sons, 1999.
- [63] S. Affatato, M. Spinelli, M. Zavalloni, C. Mazzega-Fabbro, and M. Viceconti, “Tribology and total hip joint replacement: Current concepts in mechanical simulation,” *Med. Eng. Phys.*, vol. 30, no. 10, pp. 1305–1317, 2008.
- [64] M. Scherge, D. Shakhvorostov, and K. Pöhlmann, “Fundamental wear mechanism of metals,” *Wear*, vol. 255, no. 1–6, pp. 395–400, 2003.
- [65] “ASTM G40-17: Standard Terminology Relating to Wear and Erosion1,” *ASTM Int.*, pp. 1–9, 2016.
- [66] D. Kopeliovich, “Lubrication regimes,” 2018. [Online]. Available: http://www.substech.com/dokuwiki/doku.php?id=lubrication_regimes. [Accessed: 25-Aug-2018].
- [67] S. M. Kurtz, “Future Clinical and Economic Impact of Revision Total Hip and Knee Arthroplasty,” *J. Bone Jt. Surg.*, vol. 89, no. suppl_3, p. 144, 2007.
- [68] Z. M. Jin, J. Zheng, W. Li, and Z. R. Zhou, “Tribology of medical devices,” *Biosurface and Biotribology*, vol. 2, no. 4, pp. 173–192, 2016.
- [69] K. L. Johnson, *Contact Mechanics*. Cambridge University Press, 1985.
- [70] S. Timoshenko and J. N. Goodier, *Theory of Elasticity*, 3rd ed. McGraw-Hill, 1982.
- [71] G. D. Ehrlich *et al.*, “Engineering approaches for the detection and control of orthopaedic biofilm infections,” *Clin. Orthop. Relat. Res.*, vol. 02418,

- no. 437, pp. 59–66, 2005.
- [72] A. F. Widmer, “New Developments in Diagnosis and Treatment of Infection in Orthopedic Implants,” *Clin. Infect. Dis.*, vol. 33, no. s2, pp. S94–S106, 2001.
- [73] “ISO 25178-1:2016 Surface texture: Areal Part 1: Indication of surface texture.” 2016.
- [74] S. Bruschi, R. Bertolini, F. Medeossi, A. Ghiotti, and E. Savio, “Case study : The application of machining-conditioning to improve the wear resistance of Ti6Al4V surfaces for human hip implants,” *Wear*, vol. 394–395, no. June 2017, pp. 134–142, 2018.
- [75] B. S. Ramamurti *et al.*, “Loci of movement of selected points on the femoral head during normal gait: Three-dimensional computer simulation,” *J. Arthroplasty*, vol. 11, no. 7, pp. 845–852, 1996.
- [76] A. Wang, “A unified theory of wear for ultra-high molecular weight polyethylene in multi-directional sliding,” *Wear*, vol. 248, no. 1–2, pp. 38–47, 2001.
- [77] A. Borruto, “A new material for hip prosthesis without considerable debris release,” *Med. Eng. Phys.*, vol. 32, no. 8, pp. 908–913, 2010.
- [78] T. Zhang, N. M. Harrison, P. F. McDonnell, P. E. Mchugh, and S. B. Leen, “A finite element methodology for wear – fatigue analysis for modular hip implants,” *Tribol. Int.*, vol. 65, pp. 113–127, 2013.
- [79] “ISO 7206-3:1988 Orthopaedic joint prostheses- Method for determination of endurance properties of stemmed femoral components of hip joint prostheses without application of torsion.” 1990.
- [80] D. T. Tsukayama, R. Estrada, and R. B. Gustilo, “Infection after Total Hip Arthroplasty,” pp. 512–523, 1996.
- [81] D. Ulutan and T. Ozel, “Machining induced surface integrity in titanium and nickel alloys : A review,” *Int. J. Mach. Tools Manuf.*, vol. 51, no. 3, pp. 250–280, 2011.
- [82] A. Maurotto and A. Roy, “Surface-roughness improvement in ultrasonically assisted turning,” *Procedia CIRP*, vol. 13, pp. 49–54, 2014.
- [83] R. A. Gittens *et al.*, “A review on the wettability of dental implant surfaces II: Biological and clinical aspects,” *Acta Biomater.*, vol. 10, no. 7, pp. 2907–2918, 2014.
- [84] Y. Lu, P. Guo, P. Pei, and K. F. Ehmann, “Experimental studies of wettability control on cylindrical surfaces by elliptical vibration texturing,” *Int. J. Adv. Manuf. Technol.*, vol. 76, no. 9–12, pp. 1807–1817, 2014.
- [85] R. Leach, *Characterisation of areal surface texture*, vol. 9783642364. 2013.
- [86] P. Damm *et al.*, “Friction in Total Hip Joint Prosthesis Measured In Vivo during Walking,” vol. 8, no. 11, pp. 1–8, 2013.
- [87] J. F. Archard, “Contact and Rubbing of Flat Surfaces,” *J. Appl. Phys.*, vol. 24, no. 8, p. 981, 1953.
- [88] W. Huang, L. Jiang, C. Zhou, and X. Wang, “Tribology International The lubricant retaining effect of micro-dimples on the sliding surface of PDMS,” vol. 52, pp. 87–93, 2012.
- [89] A. A. G. Bruzzone and H. L. Costa, “Functional characterization of structured surfaces for tribological applications,” *Procedia CIRP*, vol. 12, pp. 456–461, 2013.
- [90] D. E. Kim, K. H. Cha, I. Sung, and J. Bryan, “Design of Surface Micro-

- structures for Friction Control in Micro-systems Applications,” *CIRP Ann. - Manuf. Technol.*, vol. 51, pp. 495–498, 2002.
- [91] U. Sudeep, R. K. Pandey, and N. Tandon, “Tribology International Effects of surface texturing on friction and vibration behaviors of sliding lubricated concentrated point contacts under linear reciprocating motion,” vol. 62, pp. 198–207, 2013.
- [92] A. K. Å and A. Elfick, “Tribology International Influence of crosslinked polyethylene structure on wear of joint replacements,” *Tribology Int.*, vol. 42, no. 11–12, pp. 1582–1594, 2009.

